2015

Thermal Efficiency Enhancement of an A/C System Using Computer Simulations

Xinyu Zhang
University of Rhode Island, xinyu_zhang@my.uri.edu

THERMAL EFFICIENCY ENHANCEMENT OF AN A/C SYSTEM USING COMPUTER SIMULATIONS

BY

XINYU ZHANG

A THESIS SUBMITTED IN PARTIAL FULFILLMENT OF THE

REQUIREMENTS FOR THE DEGREE OF

MASTER OF SCIENCE

IN

MECHANICAL ENGINEERING

UNIVERSITY OF RHODE ISLAND

2015

MASTER OF SCIENCE THESIS

OF

XINYU ZHANG

APPROVED:

Thesis Committee:

Major Professor Zongqin Zhang

D.M.L. Meyer

K. Wayne Lee

Nasser H. Zawia

DEAN OF THE GRADUATE SCHOOL

UNIVERSITY OF RHODE ISLAND

2015

ABSTRACT

Effects of airflow maldistribution in a prototype V-shaped evaporator (Model CAD501) for an air-conditioning (A/C) system were investigated using computer simulations in this study. The configuration of the fin-and-tube heat exchanger was first simplified into a 30-channel air flow passages, and velocity profiles of air flowing through the simplified heat exchanger passages were obtained using Computational Fluid Dynamics (CFD) software ABAQUS. The performance of the A/C system was then evaluated using thermodynamics software Engineering Equation Solver (EES) based on the velocity distribution provided by the CFD simulation. Methodologies are proposed to solve the problems associated with the airflow maldistribution. Preliminary experiments were conducted to qualitatively verify some of the computer simulations and results. It was found that the airflow maldistribution would reduce the Coefficient of Performance (COP) and cooling capacity of the A/C system and this reduction could be recovered by the proposed solutions.

ACKNOWLEDGMENTS

I would like to express special gratitude to the following people and program.

The research of the thesis would not be possible without the invaluable advisory and support from my major professor, Prof. Zongqin Zhang. I would also like to thank the Nanjing Canatal Air-conditioning Electrical & Mechanical Co,. Ltd for the research topic and experimental support. I would also like to thank the 3+X program jointly offered by the University of Rhode Island (URI) and Zhejiang University (ZJU) as well as its director Dr. Sigrid Berka and Mr. Jian Luo for the precious opportunity to start my Master's study at URI.

I am grateful to my friends Jun Yan and Brittany Durgin who helped me with the formatting and grammar in this thesis work. I owe many thanks to my friends Chuanxin Zhu, Xiaonan Dong, Hanyi Zhou and Tingchia Liu for their company and encouragements.

Finally, I wish to thank my parents Yidong Zhang, Ping Chen and my brother Xinhan Zhang for their love and encouragement, without whom I would never have enjoyed my life.

TABLE OF CONTENTS

Page

Page

LIST OF TABLES

LIST OF FIGURES

CHAPTER 1

Introduction

The air conditioning system (A/C system) is crucial to modern life. It is widely used in both domestic and industrial worlds. As the old saying goes, every coin has two sides; while the A/C system brings us comfort, usage is associated with problems of energy consumption and environmental pollution. Although it is not feasible to eliminate the consumption of energy, an enhancement of energy efficiency is viable.

1.1 World Energy Problem

The Statistical Review of World Energy 2015 Report produced by British Petroleum (BP plc.) gives us a good overview of the current energy problem in the world. The review of 2014 in the report concludes, "Global primary energy consumption decelerated sharply in 2014, even though global economic growth was similar to 2013." While this seems to be good news, it actually is not. On the one hand, consumption increased for all fuels, reaching record levels for every fuel type except nuclear power. On the other hand, production increased for all fuels except coal. For oil and natural gas, global consumption growth was weaker than production. Therefore, the deceleration of primary energy consumptions means we are consuming more energy and doing it faster than ever. The emerging economies continued to dominate the growth in global energy consumption. China (+2.6%) and India (+7.1%) recorded the largest national increments to global energy consumption. A second consecutive year of robust US growth (+1.2%) was also reported.

Energy consumption of A/C systems plays a big role in this worldwide problem. Industrially, with the rapid development of cloud computing technology, the

energy consumption of the global data centers is getting more critical. A study (Jonathan et al. 2011 [1]) shows that electricity used in global data centers in 2010 likely accounted for between 1.1% and 1.5% of total electricity usage. Specifically for the US, that number was between 1.7% and 2.2%. The A/C system accounts for around 37% of the data center energy consumption. As you can see, the data centers consist of just one small piece of this puzzle affecting the whole industry that uses A/C systems. Domestically, air conditioning is also very common in the United States. A survey conducted by the US Census Bureau says that in the United States, 88% of new single-family homes constructed in 2011 included air conditioning, ranging from 99% in the South to 62% in the West.

1.2 Air-conditioning (A/C) System

In general, air conditioning (A/C) is used in order to control the temperature of a room or space to be more comfortable for those residing in it, particularly in a sweltering environment. The drop in temperature is achieved through a refrigeration cycle, wherein four separate processes combine in order to draw heat out of the occupied space and displace it to an outside area.

Figure 1 shows the T-s (temperature-entropy) diagram of an ideal vapor-compression refrigeration cycle. The most commonly used cycle for A/C system, the vapor-compression refrigeration cycle, consists of four processes:

1-2 Isentropic (constant entropy) compression in a compressor; 2-3 Isobaric (constant pressure) heat rejection in a condenser; 3-4 Irreversible isenthalpic (constant enthalpy) throttling in an expansion valve; 4-1 Isobaric (constant pressure) heat absorption in an evaporator.

As shown in Figure 2, there are four main components comprising a typical vapor-compression refrigeration cycle: compressor, condenser, expansion valve and evaporator. Typically, the evaporator is placed in an indoor area to be refrigerated

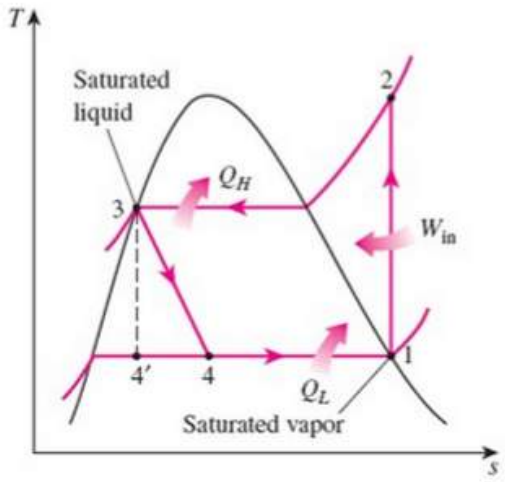

Figure 1. The T-s Diagram of an Ideal Vapor-compression Refrigeration Cycle (Yunus et al. 2011 [2])

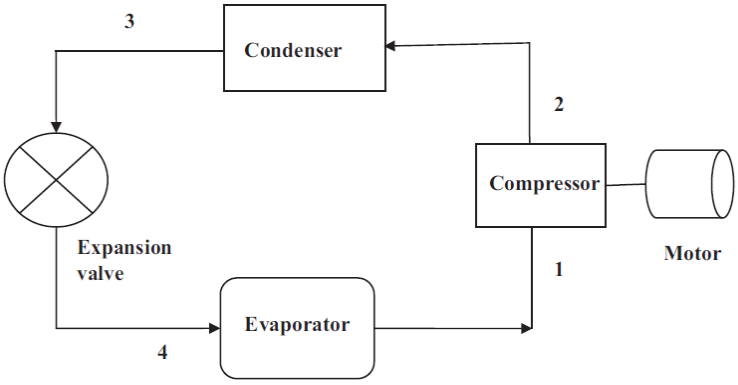

Figure 2. Schematic Diagram of Vapor-compression Refrigeration System (Ahamed et al. 2011[3])

and the condenser is placed in an outdoor space so that the refrigeration cycle takes away heat from the indoor area and rejects the heat to the outdoor space. The compressor is the only component which does work on the A/C system. In an ideal vapor-compression cycle, the refrigerant enters the compressor at state 1 and leaves at state 2. Refrigerant at the saturated-vapor-state is compressed isentropically from a low evaporator pressure to a relatively high condenser pressure. After the compression, the temperature of the refrigerant increases from the low evaporating temperature to a much higher temperature than the surrounding space. Then the refrigerant enters the condenser at state 2 and exits at state 3. The refrigerant condenses from a saturated vapor to a saturated liquid by releasing heat to the surroundings. After that, the refrigerant is throttled through the expansion valve from state 3 to state 4. The irreversible process takes its temperature down from above the outdoor temperature to below the indoor temperature. After all, the refrigerant enters the evaporator at state 4 and exits at state 1. The refrigerant completely evaporates from a low-quality saturated mixture to a saturated vapor by absorbing heat from the refrigerated indoor space. The cycle is completed as the refrigerant reenters the compressor from the evaporator. The heat transfer for internally reversible processes is expressed as the area under the process curve on the T-s diagram. Consequently, the area under the process curve 4-1 represents the heat absorbed by the refrigerant in the evaporator and the area under the process curve 2-3 represents the heat rejected in the condenser.

Figure 3 shows the P-h (pressure-enthalpy) diagram of an ideal vapor-compression refrigeration cycle which is another commonly used diagram in the analysis of vapor-compression refrigeration cycles.

It is shown that the evaporating and condensing processes appear as two horizontal lines (constant pressure lines) and the heat transfer in the condenser and

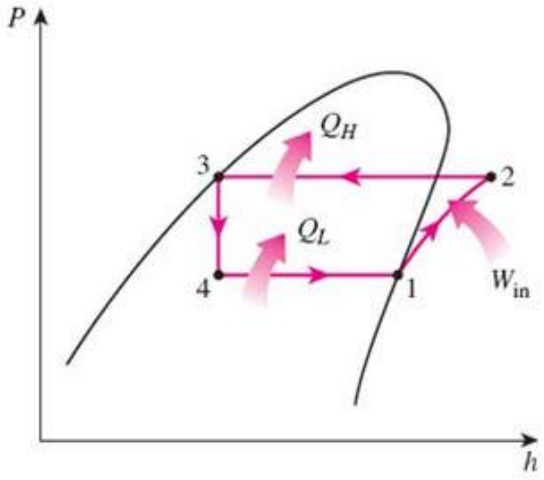

Figure 3. The P-h Diagram of an Ideal Vapor-compression Refrigeration Cycle (Yunus et al. 2011[2])

the evaporator is proportional to the lengths of the corresponding process curves 2-3 and 4-1. The throttling process appears as a vertical line on the diagram. The ideal vapor-compression refrigeration cycle is an internally irreversible cycle due to the involvement of the irreversible throttling process. The vapor-compression refrigeration can be analyzed as steady-flow processes since all four components constructing the refrigeration cycles are steady-flow devices. The kinetic and potential energy changes of the refrigerant are negligible since they are relatively small to the work and potential energy changes of the refrigerant. Then the steady flow energy equation on a unit-mass basis reduces to Equation (1),

$$(q_{in} - q_{out}) + (w_{in} - w_{out}) = h_e - h_i \tag{1}$$

where q_{in} is input heat transfer per unit mass; q_{out} is output heat transfer per unit mass; w_{in} is work input; w_{out} is work output; h_e is the specific enthalpy output; h_i is the specific enthalpy input.

No work is involved in the condenser and the evaporator since only heat transfers are conducted in them. In addition, the compressor can be approximated as adiabatic. Then the Coefficient of performance (COP) of refrigerators operating

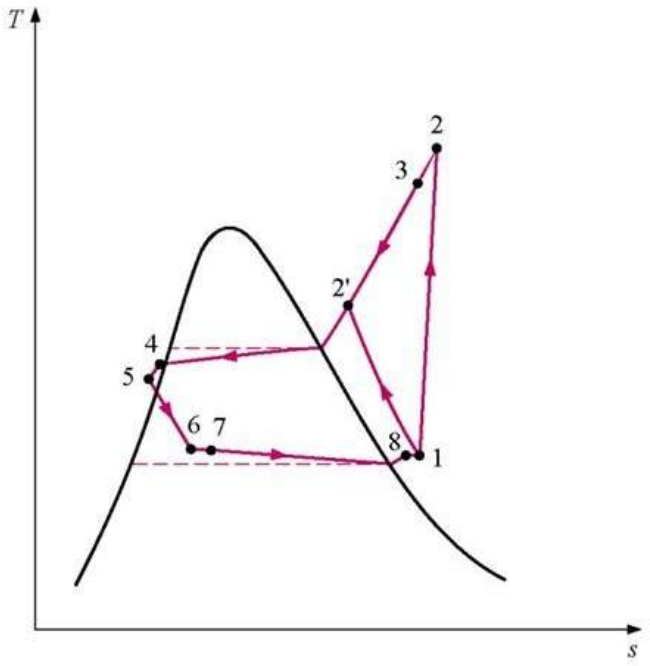

Figure 4. The T-s Diagram of an Actual Vapor-compression Refrigeration Cycle (Yunus et al. 2011[2])

on the vapor-compression refrigeration cycle can be expressed as Equation (2),

$$COP = \frac{q_L}{w_{in}} = \frac{h_1 - h_4}{h_2 - h_1} \tag{2}$$

where q_L is heat transfer per unit mass with low-temperature body; win_{in} is work input; h_1 is the enthalpy at state 1; h_2 is the enthalpy at state 2; h_4 is the enthalpy at state 4. Due to the irreversibility that occurs in various components of the cycle, an actual vapor-refrigeration cycle differs from the ideal one in several ways. The irreversibility is normally triggered by two factors: the fluid friction which causes pressure drops and heat transfer to or from the surroundings. Figure 4 shows the T-s (Temperature-entropy) diagram of an actual vapor-compression refrigeration cycle.

In the ideal cycle, the state 1 of the refrigerant leaves the evaporator and enters the compressor as saturated vapor. In practical use, however, it is a challenge

to precisely control this state of the refrigerant. To simplify the problem, an overdesign is used in order to slightly superheat the refrigerant to prevent damage to the compressor. The design of superheating makes sure that the refrigerant is completely evaporated before it enters the compressor. In practical use, there could be a considerable pressure drop caused by fluid friction and heat transfer from the surroundings to the refrigerant due to the fact that the pipeline, which connects the evaporator to the compressor, is normally very long. The specific volume of the refrigerant is increased by the combination of superheating, heat gained in the connecting pipeline, and pressure drops in the evaporator and the connecting line. As a result, the total cooling capacity of the A/C system decreases since the mass flow rate of refrigerant is inversely proportional to the specific volume. In the ideal cycle, the compression process is isentropic. However, the entropy of the refrigerant may be increased or decreased due to the involvement of frictional losses which increase the entropy, and heat transfer, which may increase or decrease the entropy depending on the direction. On the T-s diagram, process 1-2 shows the increase and process 1-2' shows the decrease of the entropy. In the case that the entropy is decreased, the compression process 1-2' is more desirable than the ideal isentropic compression process due to the reduction of the specific volume of the refrigerant which cause a decrease in work input requirements. In the ideal vapor-compression refrigeration cycle, the state 3 where the refrigerant leaves the condenser is assumed to be saturated liquid at the compressor exit pressure. In practical use, the pressure drops in the condenser and the long pipelines connecting the condenser to the compressor and to the expansion valve are inevitable. Similar to the case of the evaporator, the desired saturated liquid status of the refrigerant is difficult to ensure at the end of the condensation process. The sub-cooling design has been applied to the condenser to make sure that the refrigerant is completely

Figure 5. A Fin-and-tube Heat Exchanger

condensed before it enters the expansion valve.

1.3 Evaporator

The evaporator is the focus of this study. It is a key component in an A/C system. The fin-and-tube heat exchanger structure is used in this evaporator design.

1.3.1 Fin-and-tube Heat Exchanger

Fin-and-tube heat exchangers consist of mechanically expanded round tubes in a block of parallel continuous fins. An example is shown in Figure 5. A schematic diagram of a simplified heat exchanger is shown in Figure 6. Fin-and-tube heat exchangers are designed to maximize heat transfer between two fluids, in this study the air and the refrigerant, with a minimum pressure drop associated with each fluid. The air flows through the fins and the refrigerant flows through the tubes, completing the heat transfer between the two fluids. The design of fin-and-tube heat exchangers requires specification of more than a dozen parameters, including but not limited to the following: transverse tube spacing, longitudinal tube spacing, tube diameter, number of tube rows, fin spacing, fin thickness, and fin type etc. The foci of this study are the problems associated with air maldistribution, thus

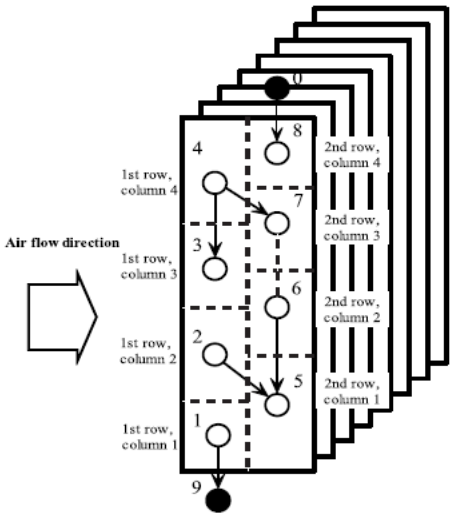

Figure 6. Schematic Diagram of a Simplified Fin-and-tube Heat Exchanger (Liu et al. 2004[4])

the design and configuration of the heat exchanger are simplified.

1.3.2 Multi-Channel Design

Figure 7 shows a multi-channel design of the evaporator with 3 individual channels. The refrigerant flows through a distributer after it exits the expansion valve and splits into 3 channels inside the evaporator. The multiple channels in parallel design is a typical design used in many A/C systems to increase the system efficiency by reducing frictional loss and increasing the refrigerant flow rate. A thermostatic expansion valve is used to control the mass flow rate of the refrigerant flowing into the evaporator by responding to the superheating temperature readings. Due to the use of the multi-channel design, the control scheme of the expansion valve can only control the overall superheating of the A/C system. Meanwhile, the distribution of refrigerant to individual channels is uncontrollable. Under the ideal conditions, mass flow rates at the refrigerant side and the airside in the evaporator are uniform and match well at every channel, and the A/C system works as designed. However, in practical use the performance of the system

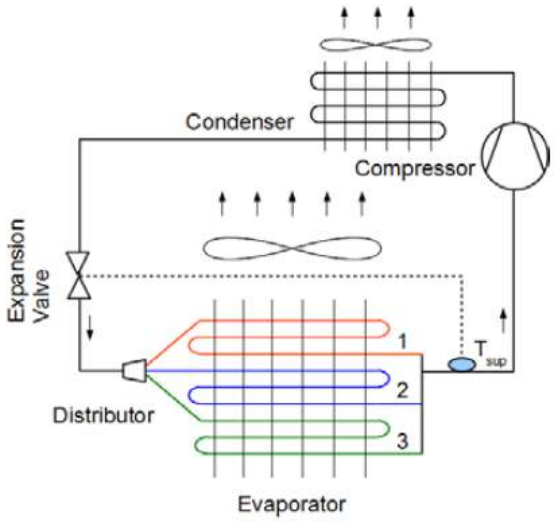

Figure 7. Three Channel Design of the Evaporator (Groll et al. 2011[5])

degrades due to problems of airside maldistribution, which is the focus of this study.

1.3.3 V-shaped Evaporator Design

Figure 8 displays the laboratory setting of a V-shaped evaporator (Model CAD501) studied in this work. Figure 9 shows the sketch with detailed exterior dimensions of the evaporator. The dimensions of the sketch are in millimeters (mm).

The returned air from the air-conditioned room is induced by a centrifugal fan into the air space from the top of the A/C unit. It flows over the evaporator surfaces and is discharged from the bottom of the A/C unit. Two fin-and-tube heat exchangers are placed symmetrically in a V-shaped configuration with an apex angle of 28 degrees.

The V-shaped design shown in Figure 8 significantly increases the heat transfer area by 413%. The design allows the maximum number of coils installed in the heat exchanger in a given space.

Figure 8. Evaporator Model CAD501 Used in Experiments

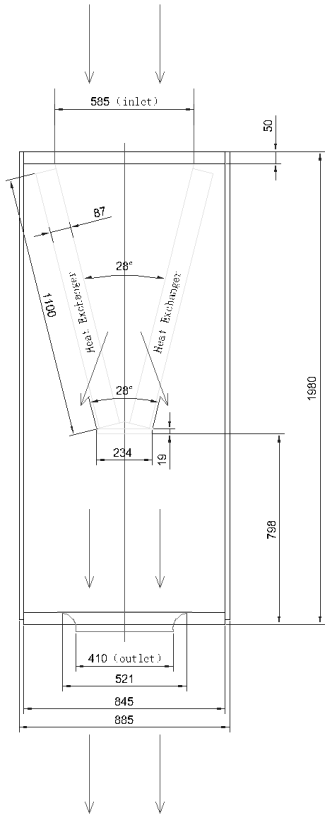

Figure 9. Dimensions of the V-shaped Evaporator Used in Study

List of References

[1] J. Koomey, "Growth in data center electricity use 2005 to 2010," *A report by Analytical Press, completed at the request of The New York Times*, p. 9, 2011.

[2] Y. A. Cengel, M. A. Boles, and M. Kanoğlu, *Thermodynamics: an engineering approach*. McGraw-Hill New York, 2011, vol. 5.

[3] J. Ahamed, R. Saidur, and H. Masjuki, "A review on exergy analysis of vapor compression refrigeration system," *Renewable and Sustainable Energy Reviews*, vol. 15, no. 3, pp. 1593–1600, 2011.

[4] J. Liu, W. Wei, G. Ding, C. Zhang, M. Fukaya, K. Wang, and T. Inagaki, "A general steady state mathematical model for fin-and-tube heat exchanger based on graph theory," *International Journal of Refrigeration*, vol. 27, no. 8, pp. 965–973, 2004.

[5] E. Groll, J. Braun, and C. Bach, "Optimizing refrigerant distribution in evaporators–final report," *California Energy Commission. Publication number: CEC-500-2013-089*, 2011.

CHAPTER 2

Literature Review

This chapter briefly reviews some of the researches published in the literature and intends to show an overview of the work done prior to this study.

Lee et al. 1997 [1] developed a theoretical model to predict the cooling capacity of finned tube evaporators with one dimensional airside maldistribution. They found that if airside maldistribution was applied, the cooling capacity for the same refrigerant and coil dropped by 9% with uniform refrigerant flow. Meanwhile, it dropped by 39% if the refrigerant side flowrate was assigned based on the pressure drop.

Payne and Domanski et al. 2002 [2] investigated the potential benefits of controlling refrigerant distribution to achieve equal exit superheats. In the experimental part of their study, they found that if the overall superheat was held constant while the individual channel superheat was allowed to vary, then the cooling capacity decreased by up to 41% and 32% for the wavy and wavy lanced fin evaporator, respectively. For non-uniform air flow tests, it was found that the capacity was recovered to within 2% of the original value if superheats were controlled to the original value. In parallel to the experiments, they used their evaporator model EVAP5 to predict possible savings in evaporator core volume if a smart distributer was used. They found that in extreme cases, the savings in core volume can be up to 40%.

In a numerical study by Lee et al. 2003 [3], non-uniform airflow profiles reduced the cooling capacity of the evaporator up to 6%.

Domanski et al. 2004 [4] proposed a computational model which used an evolutionary algorithm to optimize evaporator circuitry for uniform and non-uniform

airflow, termed as ISHED (intelligent system for heat exchanger design). It was found that for a 3 bank evaporator with 12 tubes each, the capacity of the design for uniform airflow operated at uniform airflow was slightly smaller than the one obtained for non-uniform airflow when operating in non-uniform airflow (both approximately 5.25 kW). The capacity of the design obtained for uniform airflow under non-uniform airflow dropped to 4.82 kW.

Domanski and Yashar et al. 2007 [5] used a newer version of ISHED to optimize evaporator and condenser circuitries for different refrigerants. For the evaporator designs, it was found that the ISHED generated design outperformed the best manually generated design for all refrigerants. For the condenser designs, it was found that the ISHED generated design performed equally well or better than the best manually generated design. They furthermore found, that for an A-type evaporator coil, as found in residential AC systems, the capacity improved by 4.2%, if the ISHED optimized circuitry was compared to the original circuitry. For this simulation, the velocity profile was based on particle velocity measurements and CFD simulation.

TJoen et al. 2006 [6] investigated the effects of airflow maldistribution on the performance of a 3 row air to water finned tube heat exchanger. Using different velocity profiles, he found that the overall heat transfer coefficient dropped by up to 8%, if a quadratic velocity profile was applied.

AbdelAziz et al. 2008 [7], pointed out that the airflow might also create a recirculation zone in the lower part of the coil. They carried out simulations of the airflow through an A-shaped evaporator using CFD (computational fluid dynamics) simulations. These recirculation zones in the coil led to a reduction in the cooling capacity since the recirculated airflow was not exchanged.

Kim et al. 2008 [8] introduced the hybrid control scheme for evaporators, sug-

gested possible balancing valves and evaluated possible performance benefits using a numerical model. Kim et al. 2008 [9] describes the modeling approach and results in a more concise form. The hybrid control scheme uses a primary expansion valve that provides most of the pressure drop and flow balancing valves in each individual channel to achieve uniform individual channel exit superheat. They numerically investigated an upstream flow balancing method, where the valves are placed between the distributor and circuit inlet, and a downstream flow balancing method, where the valves are placed at the exit of each channel. They found that the downstream flow balancing method leads to a larger degradation of COP and cooling capacity for air flow distribution factors of 0.9 to 0.7. For the upstream flow balancing method, they found that most of the performance degradation caused by uneven airside flow was recovered when individual circuit superheats were balanced. Specifically, for an air distribution factor of 0.6, capacity degraded by about 6% and COP by about 4% without balancing superheats. If the upstream flow balancing method was applied, most of the losses were recovered.

Kim et al. 2009 [10] explain the model used in Kim et al. 2008 [13] in greater detail. Kim et al. 2009 [11] investigates additional cases of maldistribution for the same model as previously described, considering R410A, R134A and R22 as refrigerants. For an air flow maldistribution factor of 0.6, corresponding to a flow distribution factor V_{C1}/V_{C2} of 0.4, they found a cooling capacity degradation of 16% and a COP degradation of 11%. They considered combinations of airside and refrigerant maldistribution. They found that for all considered cases, most of the capacity and COP degradation was recovered, if the upstream flow balancing method is applied.

Brix et al. 2009 [12] studied maldistribution in an R134a mini-channel evaporator for an automotive air-conditioning system. Both inlet vapor quality and

airflow non-uniformities were investigated numerically with simplified two-channel geometry. When only liquid entered into channel 2 and the remaining mixture entered channel 1, the cooling capacity was reduced by 23%. When the air velocity across channels 1 and 2 were 2.24 m/s and 0.96 m/s, the cooling capacity decreased by 19%.

Kaern et al. 2009 [13] described a simulation model for air conditioning systems, which uses a two-pass evaporator to study the effects of maldistribution. They considered airside flow velocity distribution using a factor $F_{air} = V_{fr,1}/V_m = 0.1$ and found the COP degradation was 38%. If the individual circuit superheats were controlled with applied airside distribution factor of 0.1, the COP degradation decreased from 38% to 7%. Their overall conclusion was that the conductance and COP reduction become significant when full evaporation is not reached in one of the circuits.

To compensate for maldistribution, a new method was evaluated in Mader et al. 2010 [14] with respect to cooling capacity and the coefficient of performance (COP). This method involved a coupled expansion and distributor device that was able to control the individual channel superheat by measuring only the overall superheat.

Kaern et al. 2011 [15] found that non-uniform airflow distribution leads to a COP reduction of up to 43.2% and quality maldistribution in the distributor leads to a COP reduction of up to 13%. Kaern et al. 2011 [21] confirmed their previous result that most of the capacity and COP degradation, for a wide range of airside maldistribution, can be recovered if the individual channel exit superheat is uniform.

In conclusion, based on the basic literature search, there has been a considerable amount of research done in the past to greatly advance our knowledge on the

problems of air flow maldistribution in the A/C system. The focus of this work is based on the particular problem of airflow maldistribution within the V-shaped evaporator designs and on the solutions to remedy this problem.

List of References

[1] J. Lee and P. A. Domanski, "Impact of air and refrigerant maldistributions on the performance of finned-tube evaporators with r-22 and r-407c," *Final Report, ARTI MCLR Project*, no. 665-54500, 1997.

[2] W. V. Payne and P. Domański, *Potential Benefits of Smart Refrigerant Distributors: Final Report*. DIANE Publishing, 2002.

[3] J. Lee, Y.-C. Kwon, and M. H. Kim, "An improved method for analyzing a fin and tube evaporator containing a zeotropic mixture refrigerant with air mal-distribution," *International Journal of Refrigeration*, vol. 26, no. 6, pp. 707–720, 2003.

[4] P. A. Domanski, D. Yashar, K. A. Kaufman, and R. S. Michalski, "An optimized design of finned-tube evaporators using the learnable evolution model," *HVAC&R Research*, vol. 10, no. 2, pp. 201–211, 2004.

[5] P. A. Domanski and D. Yashar, "Application of an evolution program for refrigerant circuitry optimization," *Proc. ACRECONF" Challenges To Sustainability*, 2007.

[6] C. T'Joen, M. De Paepe, and F. Vanhee, "Heat exchanger behavior in non uniform flow," *Experimental heat transfer*, vol. 19, no. 4, pp. 281–296, 2006.

[7] O. Abdelaziz, V. Singh, V. Aute, and R. Radermacher, "A-type heat exchanger simulation using 2-d cfd for airside heat transfer and pressure drop," 2008.

[8] J. Kim, J. Braun, and E. Groll, "Optimizing refrigerant distribution in evaporators," *Final Report ARTI-06040. Air-Conditioning and Refrigeration Technology Institute, Arlington, VA, USA*, 2008.

[9] J. Kim, J. E. Braun, and E. A. Groll, "Analysis of refrigerant flow distribution in evaporators," 2008.

[10] J.-H. Kim, J. E. Braun, and E. A. Groll, "A hybrid method for refrigerant flow balancing in multi-circuit evaporators: Upstream versus downstream flow control," *international journal of refrigeration*, vol. 32, no. 6, pp. 1271–1282, 2009.

[11] J.-H. Kim, J. E. Braun, and E. A. Groll, "Evaluation of a hybrid method for refrigerant flow balancing in multi-circuit evaporators," *international journal of refrigeration*, vol. 32, no. 6, pp. 1283–1292, 2009.

[12] W. Brix, M. R. Kærn, and B. Elmegaard, "Modelling refrigerant distribution in microchannel evaporators," *International Journal of refrigeration*, vol. 32, no. 7, pp. 1736–1743, 2009.

[13] M. R. Kærn, B. Elmegaard, and L. F. S. Larsen, "Effect of refrigerant maldistribution in fin-and-tube evaporators on system performance," in *50th International Conference of Scandinavian Simulation Society*, pp. 315–322.

[14] G. Mader, C. Thybo, and H. Rasmussen, "An electronic expansion valve with automatic refrigerant distribution control," *Kurzfassungen. Deutsche Kälte-Klima-Tagung 2010*, 2010.

[15] M. R. Kærn, W. Brix, B. Elmegaard, and L. F. S. Larsen, "Performance of residential air-conditioning systems with flow maldistribution in fin-and-tube evaporators," *international journal of refrigeration*, vol. 34, no. 3, pp. 696–706, 2011.

CHAPTER 3

Methodology

Refrigerant flow in an A/C system is interactive and dynamic. Because the cooling load is constantly changing for a typical A/C system, refrigerant flow control devices such as the thermostatic expansion valve are necessary to regulate the flow rate of the refrigerant. The thermostatic expansion valve is a precision device, which is designed to regulate the rate at which liquid refrigerant flows into the evaporator with high evaporator efficiency while preventing excess liquid refrigerant from entering the compressor. Most thermostatic expansion valves are adjustable and designed to respond to the refrigerant superheating measured at the manifold of the evaporator where the streams of refrigerant from different flow passages are merged. About 5°C to 15°C of superheating is usually maintained. When the valve opening enlarges, the flow rate of refrigerant increases and the A/C capacity is enhanced. Meanwhile, the change of the flow rate causes a chain of operation parameter changes including a change, mean flow velocity, a pressure drop across the valve and an evaporating temperature of the evaporator. The constant expansion and shrinking of the valve opening creates a dynamic refrigerant flow and the associated changes of the system performance; as such, these dynamic processes are difficult to track.

As discussed in the literature review, most studies on the topic of refrigerant maldistribution are conducted experimentally. The objective of this study, however, is to use computational simulations to investigate the influence of air flow maldistribution on the A/C system performance, as well as to seek possible solutions to overcome the problem and enhance system efficiency. The results of the computer simulation are qualitatively verified by the experimental measurements.

The focus of the study is on the system with V-shaped evaporators.

Since the refrigerating process is dynamic and interactive, many factors work simultaneously in practical use. It is difficult to isolate the individual factor that influences system performance during refrigerant maldistribution using experimental methods. With computational simulations, we can theoretically isolate these individual factors and focus on the dominant factors that affect system performance. The computational simulations consist of three parts: 1) autoCAD modeling of a V-shaped evaporator; 2) Computational Fluid Dynamics (CFD) simulations on the evaporator; and 3) Engineering Equation Solver (EES) modeling of the A/C system. First, a 2-D model of the evaporator air space configuration is sketched using autoCAD (version J.51.0.0, Autodesk Inc.). Secondly, detailed velocity and pressure distribution profiles are obtained using the CFD software, ABAQUS (Student edition 6.14-2, Dassault systems), using the autoCAD generated configuration. Finally the simulations and calculations are conducted using thermodynamics software EES (Academic Commercial V9.942-3D, F-Chart Software) based on the velocity distribution provided by the CFD simulation.

3.1 CAD Modeling of the Evaporator

The evaporator is the key module in the A/C system which provides the cooling capacity by evaporating of refrigerant at a low predetermined pressure. It is the very same component in which the problems of refrigerant maldistribution induced by airflow maldistribution occurs. As discussed in the introduction section, the V-shaped evaporator configuration provides the maximum heat transfer surface area within a given space. However, this configuration causes the uneven distribution of airflow.

Since the subject of CFD simulations is the air flow patterns over the evaporator, the sketch to be generated from the evaporator design is the air space design

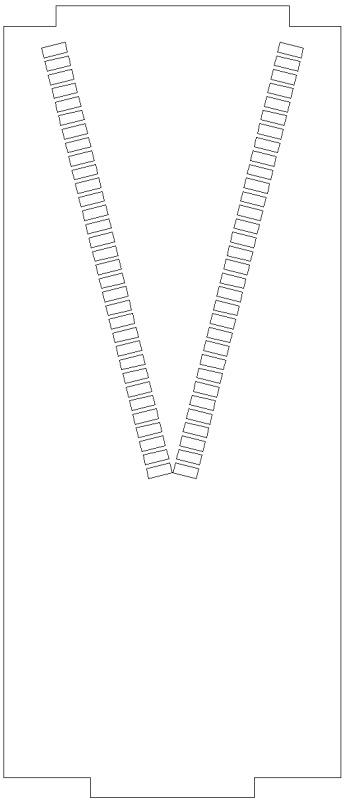

Figure 10. The 2-D Sketch of the Evaporator Air Space

of the evaporator. The main purpose of the CFD study is to qualitatively, rather than quantitatively, analyze the effect of air maldistribution on the COP of the A/C system. The original configurations and sizes of the tubes-and-fins structure are dense, small, detailed and direct computer modeling. Therefore, they require a considerable amount of computer memory, CPU time and software resources, which would cause problems in our CFD simulations. Therefore, the complicated 3-D air flow passage within the heat exchanger made of numerous finned coils is simplified to 30 2-D parallel placed straight passages. Figure 10 shows the 2-D sketch of the evaporator air space generated from the original design. Each block inside the frame represents the simplified and integrated groups of evaporator coils with fins.

3.2 CFD Simulations on Airflow through the Evaporator

In this study, the steady state CFD simulations are conducted using CFD software ABAQUS which allows users to define all the dimensions, properties and boundary conditions in the visual interfaces. Using ABAQUS, the geometry is meshed into pieces of elements, and the CFD simulations are run under two governing equations as follows.

$$\frac{\partial \rho}{\partial t} + \nabla \cdot \left(\rho \vec{V}\right) = 0 \tag{3}$$

$$\rho \frac{d\vec{V}}{dt} = \rho d\vec{f} + \nabla \cdot \tau - \nabla p \tag{4}$$

Equation (3) is the conservation of mass equation, indicating that the reduction rate of the mass in the control body is equal to the rate of mass flowing out of the control body. Since the simulations are conducted in a steady state, the differential of time can be eliminated. Since the velocities of airflow inside the evaporator air space are relatively low, the Reynolds number in each air passages are small and the airflow can be considered as incompressible flow, thus we can get equation (5). Substitute Equation (5) into Equation (3), then we can get the conservation of mass equation demonstrated by Equation (6).

$$\frac{\partial u}{\partial x} + \frac{\partial v}{\partial y} + \frac{\partial w}{\partial z} = 0 \tag{5}$$

Equation (4) is the Navier-Stokes Equation which was developed from the conservation of momentum equation, indicating that the flowing of fluids is determined by mass force, viscous shearing stress and pressure together. In this study the air is a Newtonian fluid so that the shearing stress can be expressed as Equation (7).

$$u\frac{\partial \rho}{\partial x} + v\frac{\partial \rho}{\partial y} + w\frac{\partial \rho}{\partial z} = 0 \tag{6}$$

$$\tau_{i,j} = \mu\left(\frac{\partial u_i}{\partial x_j} + \frac{\partial u_j}{\partial x_i}\right) + \lambda\delta_{ij}\left(\nabla \cdot \vec{V}\right), \lambda = -\frac{2}{3}\mu \tag{7}$$

To solve a specific problem in fluid mechanics, several initial and boundary conditions must be defined. These conditions could be the velocity or pressure. Boundary conditions define the parameters at the boundaries of the flow field. In this study, the CFD simulations are run on the air space of the working evaporator. The energy equation is not solved in the simulation.

In ABAQUS the Spalart-Allmaras Turbulence Model is used to simulate the turbulent flow. The Spalart-Allmaras model is a transport equation model for the eddy viscosity. The differential equation is derived by using empiricism and arguments of dimensional analysis, Galilean invariance and selected dependence on the molecular viscosity. The one equation model is given by Equation (8). In this equation, $\tilde{v}$ is the Spalart-Allmaras turbulence variale; v is the molecular dynamic viscosity; $\tilde{S}$ is the modified vorticity magnitude; d is the distance from the field point to the nearest wall; and the other symbols are constants. The boundary conditions are required to define the turbulent kinematic viscosity at the inlet and walls. More details about the Spalart-Allmaras Turbulence Model and other turbulence models can be seen in Rumsey et al. 2015[1].

$$\frac{\partial \tilde{v}}{\partial t}+u_j\frac{\partial \tilde{v}}{\partial x_j}=c_{b1}\left(1-f_{t2}\right)\tilde{S}\tilde{v}-\left[c_{\omega 1}f_\omega-\frac{c_{b1}}{\kappa}f_{t2}\right]\left(\frac{\tilde{v}}{d}\right)^2+\frac{1}{\sigma}\left[\frac{\partial}{\partial x_j}\left(\left(v+\tilde{v}\right)\frac{\partial \tilde{v}}{\partial x_j}\right)+c_{b2}\frac{\partial \tilde{v}}{\partial x_i}\frac{\partial \tilde{v}}{\partial x_i}\right] \tag{8}$$

In ABAQUS, the air space was meshed into small pieces. It solves the pressure field and velocity distribution using these two governing equations, and the initial and boundary conditions by using numerical iteration from piece to piece.

Results of air pressure and velocity distribution over the heat exchanger are displayed using pressure contours and velocity vectors, respectively using ABAQUS software.

Figure 11 shows the meshing of the evaporator air space. The mesh size of the

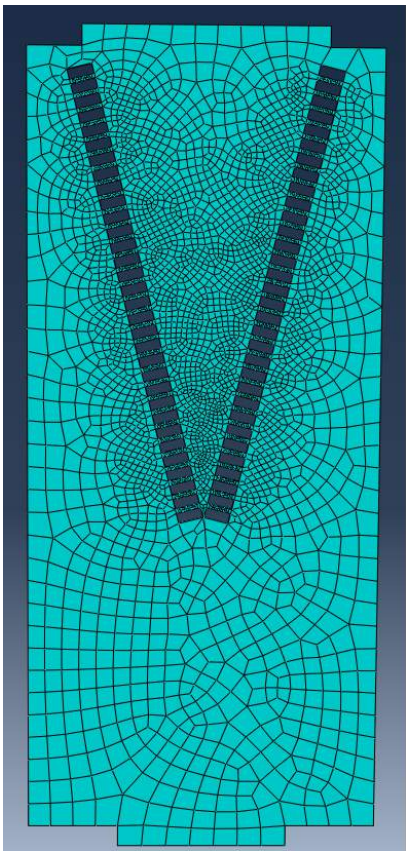

Figure 11. Meshing of the Evaporator Air Space

elements inside the air passages is about 10 times smaller than the size of the ones outside to ensure the accuracy of the velocity iterations. Grid tests were conducted to ensure that the velocity profiles obtained from the simulation are independent of the grid size.

3.3 EES Modeling

EES (Engineering Equation Solver) is a general equation-solving program that can numerically solve nonlinear algebraic and differential equations. EES has a high accuracy thermodynamic and transport property database for hundreds of substances in a manner that allows it to be used with equation-solving capability. The detailed introduction on EES software can be seen in Klein et al. 2015 [2].

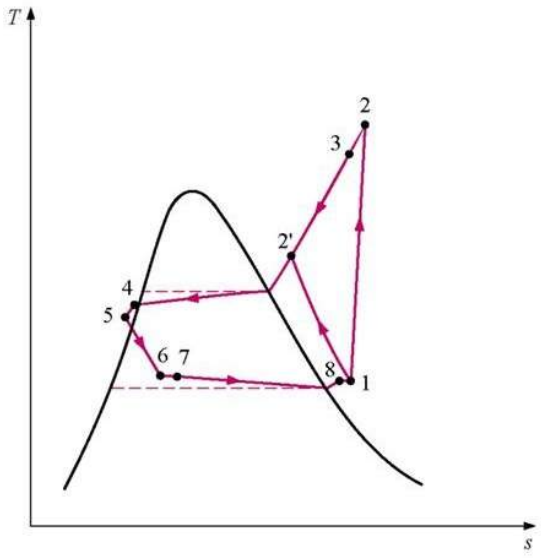

Figure 12. The T-s Diagram of an Ideal Vapor-compression Refrigeration Cycle (Yunus et al. 2011 [3])

3.3.1 EES Modeling of the A/C System

Figure 12 shows the Temperature-entropy (T-s) diagram of an actual vapor-compression refrigeration cycle. The simulation of the A/C system starts from the tracking of the state of refrigerant at different points of the refrigeration cycles. The effects of pressure drops due to frictional flow, the gravitational effects, the isentropic and the volumetric efficiency of the compressor are not included in EES models. As introduced in Section 1.2, the relationships between the parameters of refrigerant in each state can be determined as follows.

State 1 to state 2 is an isentropic compression process as the refrigerants is compressed from low pressure to high pressure by the compressor, where entropy values before and after compression are equal, i.e. $s_2 = s_1$.

State 2 to state 3 is an isobaric process isobaric (constant pressure) as the refrigerant flows through the condenser, changing from the state of high pressure superheated vapor to the subcooled liquid. The pressure values before and after the condenser are equal, i.e. $P_3 = P_2$.

State 3 to state 4 is an irreversible isenthalpic process (constant enthalpy), as the refrigerant flows through the expansion valve, and the enthalpy values before and after the thermostatic expansion valve are equal, i.e. $h_3 = h_4$. The flow is choked passing through the expansion valve from a state of high pressure liquid to a state of low pressure saturated liquid-vapor mixture.

State 4 to state 1 is again an isobaric process (constant pressure) as the refrigerant flows through the evaporator changing from the saturated liquid-vapor mixture to the state of low pressure superheated vapor. The pressure values across the evaporator are equal, i.e. $P_1 = P_4$. The heat energy released from the circulating air flow, through the fin-and-tube structured heat exchanger, is absorbed by the evaporating refrigerant inside the evaporator. In this EES modeling work, the thermodynamic properties of the refrigerant are typically described by the following commonly used thermodynamics parameters: temperature T, pressure P, entropy s, enthalpy h, specific volume v and saturated liquid-vapor mixture quality x. According to the state principle, in a simple compressible system such as the A/C system studied in this work, two independent values will determine the values of the rest. Some key temperature values are determined by the operating condition of the A/C system, such as evaporating temperature T_{evap}, condensing temperature T_{cond}, low pressure vapor superheating temperature T_{suph} and high pressure liquid subcooling temperature T_{subc}. In an ideal thermodynamic A/C cycle, all the parameters can be obtained by combining the A/C operating temperature conditions and using state principles. The calculation of the performance of the A/C system includes total cooling capacity, the input work of the compressor and the coefficient of performance. These parameters can be defined as: The total cooling capacity Q

$$\dot{Q} = \dot{m}\,(h_1 - h_4) \tag{9}$$

The input power of the compressor

$$\dot{W} = \dot{m}\,(h_2 - h_1) \tag{10}$$

And the coefficient of performance of the A/C system

$$COP = \frac{\dot{Q}}{\dot{W}} = \frac{h_1 - h_4}{h_2 - h_1} \tag{11}$$

The mass flow rate, $\dot{m}$, of the A/C system is calculated as density (at the exit of the evaporator) multiplied by the volumetric flow rate of the compressor. The volumetric rate of the compressor is kept as a constant in EES modeling, while the density of refrigerant varies with the A/C operating conditions.

It is assumed in EES modeling that the maldistributed air flow and refrigerant flow mainly affect the performance of the evaporator; so that the refrigerant status in other components of the A/C system is not affected.

3.3.2 EES Modeling of the Evaporator

Since the rest of the components are assumed to work in ideal conditions in this study, the performance of the evaporator will determine the overall performance of the A/C system.

A typical evaporator of an A/C system consists of a large number of finned tubes. These tubes are usually evenly divided into many groups, connected one by one with 180 degree bends to form many back-and-forth flow channels. Figure 13 below shows a simplified evaporator model used by Kaern et al. 2009 [4]. In this model, the evaporator has only two flow channels, with each channel consisting of only one pipe. Liquid refrigerant passes through the distributor, gets evenly distributed into two flow channels, and evaporates inside the heat exchanger (releasing heat to the passing air stream). The vapor refrigerant then merges at the end of the evaporator (evaporator manifold) and the refrigerant is returned to the compressor.

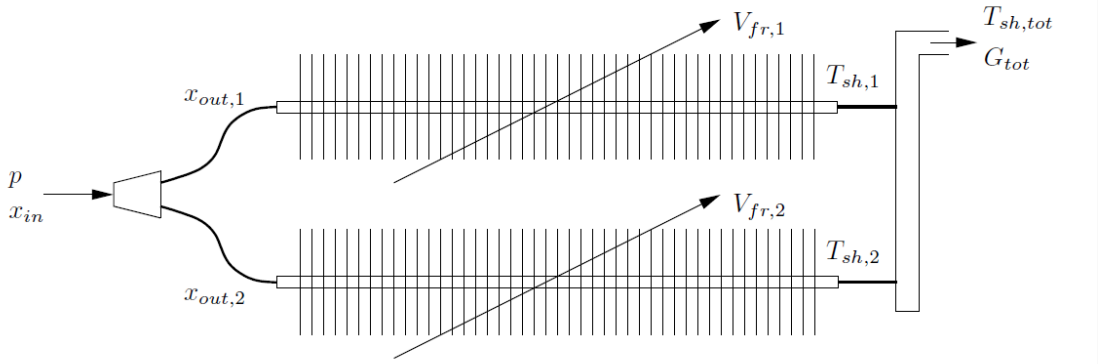

Figure 13. Sketch of the Model Setup (Kaern et al. 2009 [4])

In a typical design, mass flow rates of the liquid refrigerant distributed to each channel are of the same value. On the other hand, the mean velocity of air flow over the surface of each refrigerant channel can vary considerably, which causes the undesired mismatch problem. Kaern et al. 2009 [4]), defined an air flow distribution parameter $F_{air} = V_{fr,1}/V_m$ to describe the air flow maldistribution, where V_f is the fractional flow velocity and V_m is the mean flow velocity. In their study, the refrigerant flow was limited to two channels. When F_{air} is unity, the air-flow is indicated to distribute equally across the two tubes. When F_{air} is zero, the air flows only across channel 1. The two-channel model represents an extreme case of air maldistribution.

Figure 14 illustrates the concept of our strategies to optimize the performance of the A/C system. Panel A of Figure 14 shows the idealized heat transfer design that mass flow rates of air and refrigerant distribute evenly along the evaporator. The rate of heat rejected from the air matches the rate of heat absorption by the evaporating refrigerant everywhere over the evaporator surface.

Panel B of Figure 14 shows a typical V-shaped evaporator design that shows the mass flow rate of refrigerant distributed evenly while the mass flow rate of air is skewed. For refrigerant regions with higher air mass flow rates where air flow is

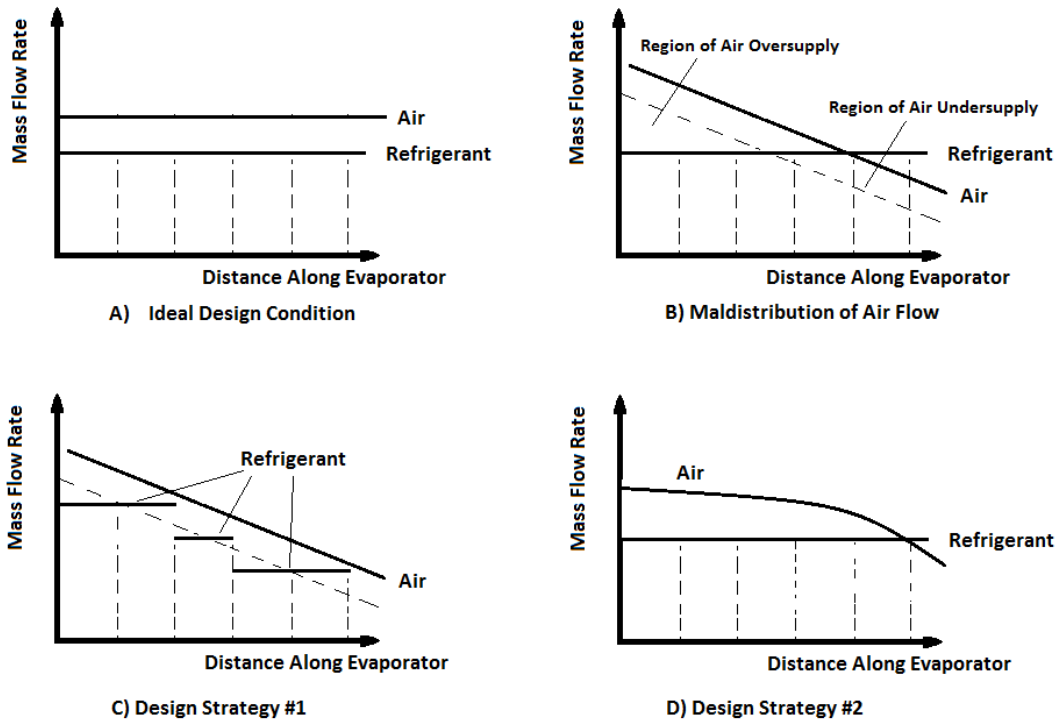

Figure 14. Heat Transfer Optimization between Air and Refrigerant

oversupplied, shown in Panel B, the refrigerant may be completely evaporated and become superheated vapor in the halfway of channel. This will provide little or zero heat transfer throughout the remaining part of the channel. Not only does the precious heat transfer surface become nonfunctional, but the superheated vapor also has a greater value of specific volume, which is associated with a larger flow velocity, a greater pressure drop, and greater pumping power. The larger pressure drop will further limit the refrigerant flow into these refrigerant superheated channels. For refrigerant channels with a lower air mass flow rate where air flow is undersupplied, shown in Panel B, the refrigerant may not completely evaporate and will become a saturated liquid-vapor mixture at the end of the evaporator. Not only are the heat transfer rates in these air-undersupplied channels not efficient, but the liquid-vapor mixture also has a lower value of specific volume, which is associated with lower flow velocity, low frictional loss and smaller pressure drops.

The lower values of the pressure drop further increase the refrigerant flow into these poor efficiency heat transfer channels. Furthermore, as the liquid-vapor mixture merges and mixes with refrigerant from all channels at the end of the evaporator (evaporator manifold), it provides low superheating false information to the thermostatic expansion valve readings. This tricks the thermostatic expansion valve to reduce the mass flow rate and lower the evaporation temperature, which is associated with the lower A/C coefficient of performance. Unstable and random mixing of hot superheated vapor with cold liquid-vapor mixture also causes a malfunction of the thermostatic expansion valve and unstable oscillating working conditions of the A/C system.

We propose two types of basic strategies to solve the problems of air maldistribution. The first type is to improve the performance of the A/C system by matching the refrigerant distribution with the existing mal-distributed air flows. The second type of strategy is to minimize the maldistribution of air flow from the source, before the air flow reaches the passage of the evaporator.

Figure 14, Panel C illustrates the design optimization Strategy #1. In this strategy, we will change the mass flow rate distribution of the refrigerant to match the skewed mass rate distribution of the air flow. This can be achieved by several methods, such as by adding additional control valves to each region or by changing the length of the refrigerant channel.

Figure 14, Panel D Panel D illustrates the design optimization Strategy #2. In this strategy, we will improve the air velocity profiles over the heat exchanger surface. This can also be achieved by several methods, such as by adding a flow-resistant filter structure or by adding a flow guide device.

As stated in chapter 3.1, in this study, the complicated, many tubes of the detailed 3-D tube-and-fin configurations of the evaporator are simplified into a

structure of 30 parallel coils for each heat exchanger. This is done in order to obtain reasonably clearer overall flow distribution of CFD simulation results.

The evaporator model developed in this study and used in the EES simulation is based on energy conservation principles. The heat loss of the air flow is equal to the absorption of heat by refrigerants in coils $\dot{Q}_{air} = \dot{Q}_L$. The energy conservation equation applies at both macro and micro scales of the evaporator. Specifically, the heat loss of the air after it flows through the evaporator is equal to the total cooling capacity the evaporator provides, and the heat loss of the air flowing through each coil is equal to the cooling capacity provided by each coil. The heat loss of the air is defined as:

$$\dot{Q}_{air} = \dot{m} C_p \Delta T = \dot{m} C_p \left(T_{in} - T_{out}\right) \tag{12}$$

where $\dot{m}$ is the mass flow rate, C_p is the specific heat capacity and $\Delta T$is the mean temperature change of the air. The mass flow rate of the air can be expressed as $\dot{m} = \rho A v$, where ρ is the density, A is a cross-section of the space the air flows through and v is the mean velocity of the air. The mass flow rate of air is directly proportional to velocity and the change of the temperature is small enough that it can be neglected. Therefore, for each coil, the heat loss of the air flows can be approximated as the linear function of mean flow velocity:

$$\dot{Q}_{air} = kv + b \tag{13}$$

where k and b are constant values to be determined by energy conservation principles. The determination of the constants k and b can be conducted by presuming that the state of the refrigerant exiting from the evaporator achieves the ideal sate under the mean velocity of the velocity profile. For each tube, the absorption of heat can be expressed as:

$$\dot{Q}_i = \dot{m} \left(h_{1i} - h_4\right) \tag{14}$$

where $\dot{m}$ is the mass flow rate of the refrigerant in each tube, h_4 is the enthalpy at the entry of the coil and h_{1i} is the enthalpy at the exit of each channel. Without a control theme on the distributor, the mass flow rate distributed into each circuit is considered to be the same.

With the velocity profiles obtained from the CFD simulations, the equations can be solved and the state of the refrigerant at the exit of the evaporator, which is marked as state 1, can be determined.

3.4 Experimental Setup

The experiments of this work are conducted in the E-cooling Laboratory of the Nanjing Canatal Air-conditioning Electrical & Mechanical Co., Ltd.

Figure 15 shows the experimental setup of the A/C system. Components shown in the picture include the V-shaped evaporator, digital thermostatic expansion valve, evaporator manifold, Copeland compressor, low pressure suction pipe between the evaporator , and the high pressure vapor discharge pipe between the compressor and the condenser. Not shown in the photo are the variable temperature controlled condensers. The components and model types used in the experiments are listed as follows:

1. A V-shaped Evaporator: Prototype CAD501;
2. A Copeland Compressor: Model VR190;
3. An air-cooled Condenser: Prototype NACD30;
4. A digital Thermostatic Expansion Valve: Model DANFOSS 15RT;
5. A variable frequency Centrifugal fan: Model EBM R3G560-RB31-71;
6. A refrigerant Distributer: Brand JingXin.

Due to time limitations of this Master's thesis work, the objective of the experimental work is to qualitatively verify the feasibility of some proposed solutions that attempt to overcome the problems associated with the maldistribution of airflow and refrigerant flow.

The pressures of the A/C system at each state were measured using a Testco differential pressure meter. The temperature of the V-shaped evaporator was monitored and recorded using a Testco infrared camera.

Due to time limitations, we used the existing set up of the laboratory. Different from the computer simulations, the position of the centrifugal fan in the experiments was changed from the top of the A/C device to the bottom. In other words, the air was induced from the bottom and flew out from the top. However, this modification to the system does not change the emergence of airflow maldistribution problem.

List of References

[1] C. Rumsey, B. Smith, and G. Huang, "Langley research center turbulence modeling resource," *http://turbmodels. larc. nasa. gov/[retrieved 13 Nov. 2015]*, 2012.

[2] S. Klein and F. Alvarado, "Ees manual," *Middleton, Wisconsin, USA*, 1999.

[3] Y. A. Cengel, M. A. Boles, and M. Kanoğlu, *Thermodynamics: an engineering approach*. McGraw-Hill New York, 2011, vol. 5.

[4] M. R. Kærn and B. Elmegaard, "Analysis of refrigerant mal-distribution: in fin-and-tube evaporators," *Danske Køledage*, pp. 25–35, 2009.

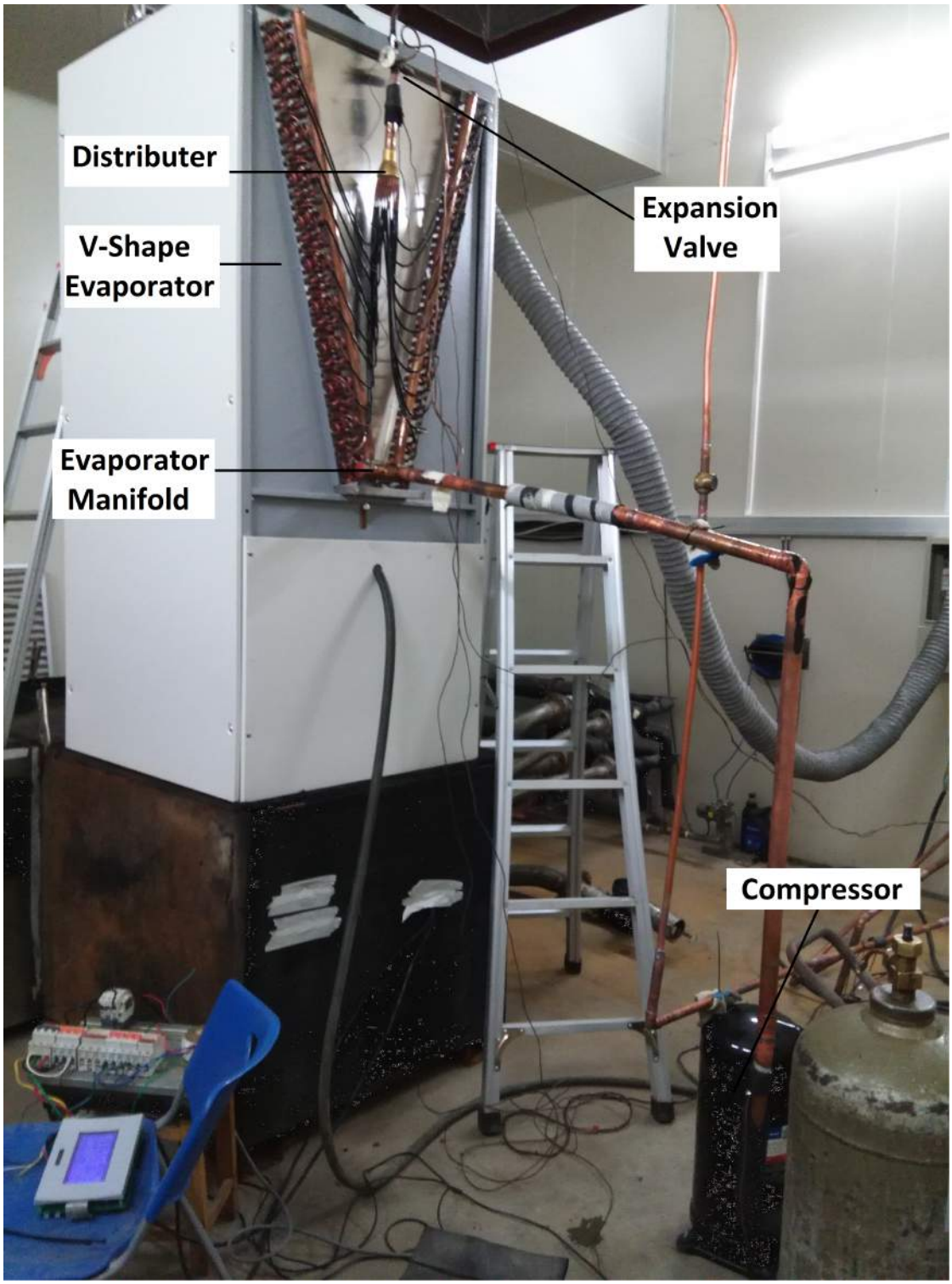

Figure 15. The Experimental Setup

CHAPTER 4

Results and Discussions

As discussed earlier, the advantage of the V-shaped evaporator design greatly increases the number of coils in a relatively small cross sectional area. However, its side effects of air maldistribution and refrigerant maldistribution is also significant.

In Section 4.1, benchmark simulations, marked as case 1 simulations, are conducted to investigate the effects of operating conditions on the performances of an ideal A/C system. The coefficient of performance COP and cooling capacity, as functions of evaporating temperature and condensing temperature are displayed. In Section 4.2, the effects of airflow maldistribution associated with the original v-shaped evaporator design, on the performance of A/C system are discussed. These studies are marked as case 2 studies. In Section 4.3, four approaches are proposed and demonstrated computationally to solve the potential maldistribution of air and refrigerant flows. These four approaches are marked as cases 3, 4, 5 and 6, respectively.

4.1 Benchmark Simulation: Thermodynamics simulations on an ideal A/C system (without air maldistribution)

The coefficient of performance, defined as COP as a function of evaporating temperature, T_{evap} , and condensing temperature T_{cond} is shown in Figure 16.

In all of these simulations, the subcooling and superheating temperatures are set to constants, T_{subc}= 5°C and T_{suph}= 10°C. These are typical values of vapor superheating at the low pressure side and liquid subcooling at the high pressure side used in many practical operations. In the simulation, the range of evaporating temperatures vary between 5°C to 15°C, condensing temperatures between 35°C to 55°C, and the computed COP value from 4.3 at $T_{evap} = 5$°C and $T_{cond} = 55$°C, to

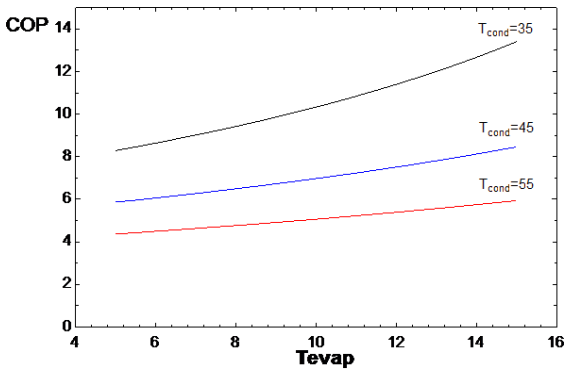

Figure 16. COP- T_{evap} Plot of an Ideal A/C System

13 at $T_{evap} = 15°C$ and $T_{cond} = 35°C$. Figure 16 shows that the COP monotonically increases with the evaporating temperature T_{evap}; and is inversely related to the condensing temperature T_{cond}. The cooling capacity (kW), Q_L, as a function of the evaporating temperature, T_{evap} , and condensing temperature T_{cond} is shown in Figure 17.

Figure 17, Q_L was plotted under the same conditions as Figure 16, COP plot with subcooling and superheating T_{subc}= 5°C and T_{suph}= 10°C, and condensing temperatures T_{cond} are set to be 35°C, 45°C and 55°C, respectively. Figure 17 shows that cooling capacity Q_L increased as the evaporator heated up, and it decreased as condensing temperature T_{cond} increased. Figure 17 shows that cooling capacity (kW), Q_L has a similar trend as well as similar magnitude of increase as COP shown in Figure 16.

The coefficient of performance, COP, as a function of the superheating, T_{suph} , is shown in Figure 18. And the cooling capacity, Q_L, as a function of the superheating, T_{suph} , is shown in Figure 19.

The COP and the cooling capacity Q_L were both plotted three times as a function of T_{suph} with condensing temperature T_{cond} 35°C, 45°C and 55°C, respectively. Since the room temperature is usually around 25°C, the subcooling temperature is set to T_{subc}= 5°C to ensure that the temperature of refrigerant

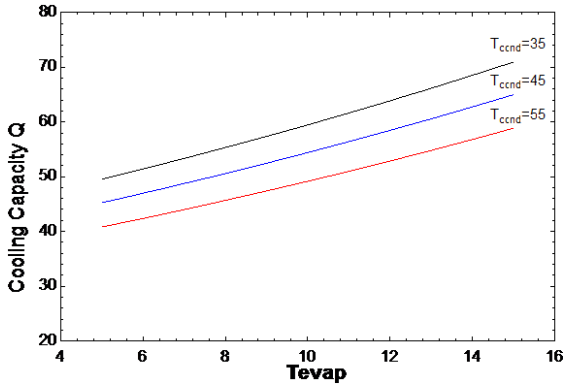

Figure 17. Cooling Capacity Q_L -T_{evap} Plot of an Ideal A/C System

Table 1. Setting of Temperature Parameters Used in This Study

Parameters	T_{evap}	T_{cond}	T_{suph}	T_{subc}
Values	5°C	45°C	10°C	5°C

exiting the condenser is above the room temperature. Similarly, the temperature of cooled air flowing out of the evaporator is about 15°C so that the evaporating temperature is usually set to T_{evap}= 5°C to make sure the evaporating temperature is below the temperature of cooled air. Figures 18 and 19 show that the COP and Q_L were both nearly independent of superheating temperature T_{suph}. It is noted that the total cooling capacity is calculated as mass flow rate multiplied enthalpy changes across the evaporator. Although the increase of superheating temperature T_{suph} increases the refrigerant cooling per unit mass flow, the superheating also increased the specific volume of the refrigerant. As a result, the mass flow rate from the compressor decreased. In other words, the effect of vapor superheating is offset by the effect of density decrease. The superheating at the exit of the evaporator is controlled to ensure that the refrigerant is fully evaporated and no wet refrigerant can enter and damage the compressor. Simulations show that effects of vapor superheating to COP and cooling capacity Q_L is negligible. Table 1 shows the settings of the temperature parameters in the simulations of case 2 to case 6. The calculation results under these temperature settings are as follows: Cooling

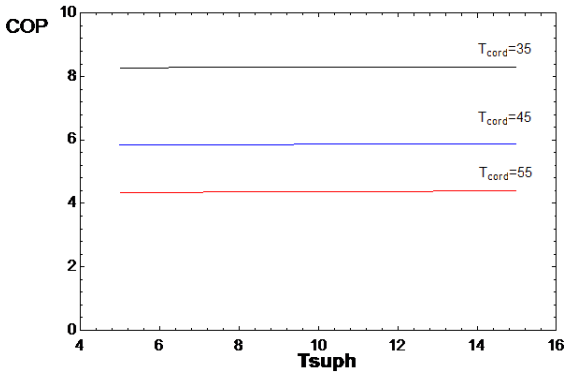

Figure 18. COP-T_{suph} Plot of an Ideal A/C System

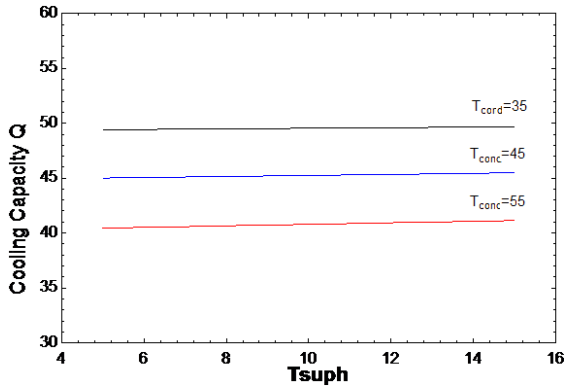

Figure 19. Cooling Capacity Q_L - T_{suph} Plot of an Ideal A/C System

capacity Q_L=45.24[kW]; Compressor Work $W_{compressor}$=7.717[kW]; Coefficient of performance COP=5.862.

The ideal A/C system under the specific temperature conditions shown in Table 1 is marked as case 1. The temperature conditions are also applied to the other cases to be discussed in the following paragraph.

4.2 Original V-shaped Evaporator Design Based Simulations

In Section 4.1, we discussed the performance of an A/C system under ideal conditions without problems associated with air maldistribution. In this Section the effects of air maldistribution caused by the original V-shaped evaporator design are studied.

4.2.1 Pressure and Velocity Distribution of the Evaporator Air Space

Figure 20 displays the computational pressure field inside the air space of a V-shaped evaporator. Air is induced into the evaporator air space by a centrifugal fan at a constant speed of 7.4 m/s at the inlet. The pressure value at the exit is set to equal to 0. The geometry of heat exchanger coils and the evaporator finned passage are simplified into 30 passages along the evaporator surface, which allow no air to flow through the boundaries.

Figure 20 shows that pressure values decrease from a high value to a low value at the exit. The pressures of air along the heat exchanger on both the inlet and outlet sides decrease as the air flows down. There are considerable pressure drops across the evaporator as demonstrated by the discontinuous display of the color changes. The pressure drop inside the air channels of the evaporator can not be displayed due to the grid resolutions. Relatively high pressure values demonstrated by the darker pressure contours at the four corners of the air space show the stagnation of the air pools at the four corners.

Figure 21 shows the velocity distribution inside the V-shaped air space of evaporator. Figure 21 indicates that most of the air induced into the evaporator air space flows through the heat exchanger, which is a designated pass. Few air flows bypass the heat exchanger. Larger velocity values occur near the entrance and exit of the air space while velocities are greatly slowed down when air flows in the flow passage of evaporator. In practical heat exchanger configurations, the narrow passage of the coil-and-fin structure creates a large resistance to the flow. The maximum velocity is found to be near the flow exit where it has the smallest cross sectional area for the flow.

Figure 22 shows the velocity distribution long the heat exchanger air passages. This is a zoomed-in figure from Figure 21, displaying the velocity distribution through the heat exchanger air passages. Flow has the highest mean velocity value at the first air flow passage and gradually reduces as the evaporator flow passages move away from the entrance at the top. The air flow distribution parameter, F_{air}, defined as the ratio of mean velocity value at local air passage to the mean velocity at the first air passage, decreases from 1 to approximately 0.6 for each passage along the heat exchanger.

4.2.2 COP and Cooling Capacity of the A/C System

Figure 23 shows the air velocity profile extracted from the CFD simulation. It clearly demonstrates the air maldistribution along the vertical direction. The velocity of air decreases monotonically as the distance further away from the entrance. The rate of flow slowing down is relatively quick for the first 10 air passages and then the decrease becomes gradual. This air velocity profile will be used as input for the EES simulation of an A/C system. As discussed in Chapter 3, the flowing of the refrigerant inside an A/C system is a dynamic and interactive process, and it is regulated by the expansion valve. In this study, the performance

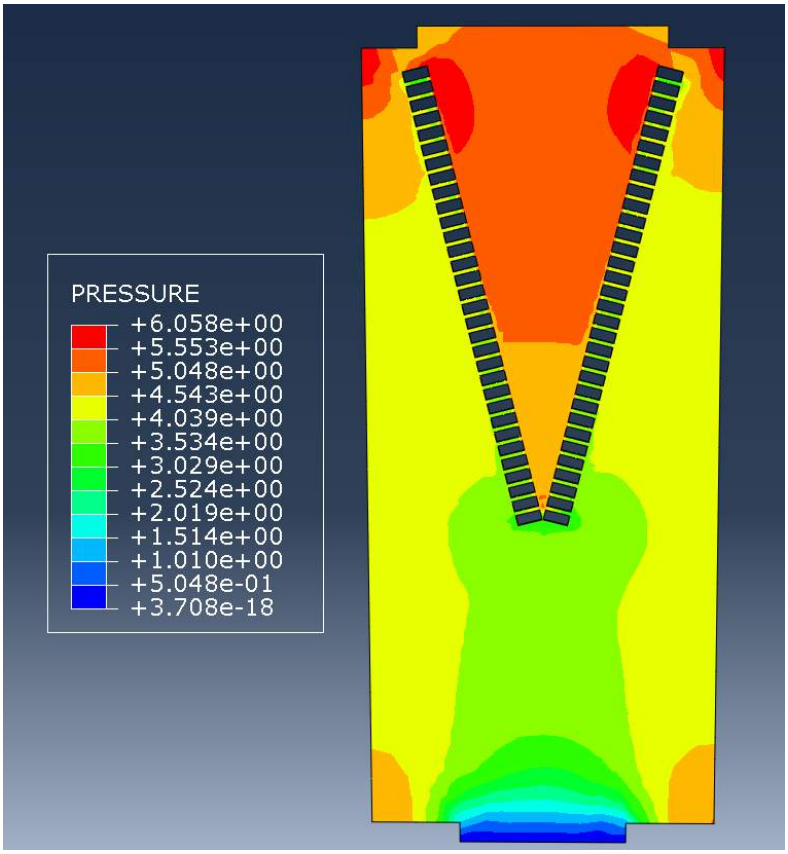

Figure 20. Pressure Distribution of Air inside the Air Space of the Evaporator

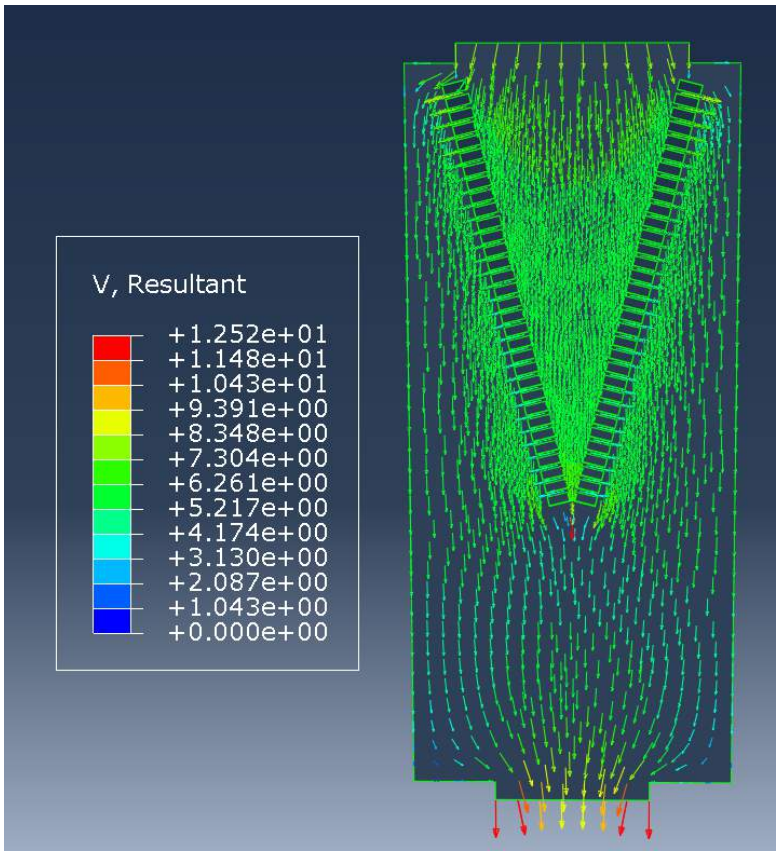

Figure 21. Velocity Distribution of Air inside the Air Space of the Evaporator

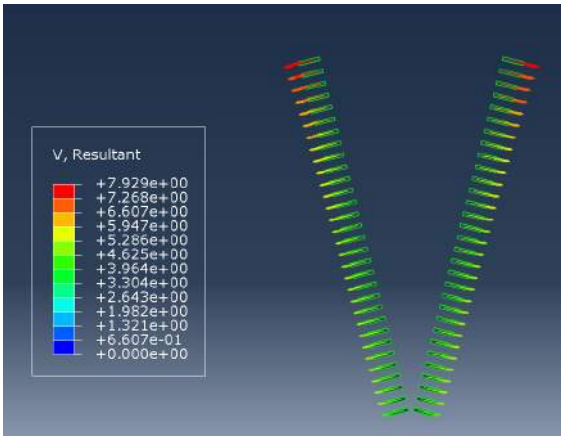

Figure 22. Velocity Distribution of Air through the Passages along the Heat Exchangers

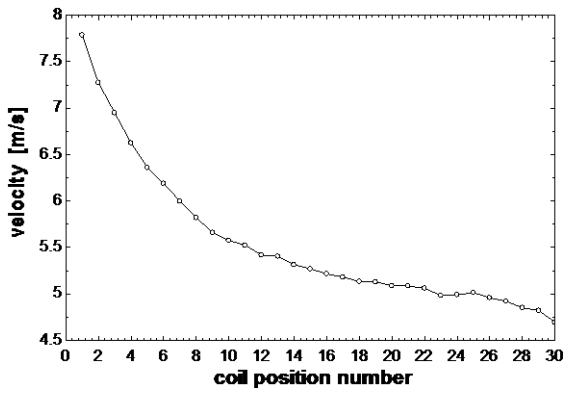

Figure 23. Velocity Plot of Air through the Passages along the Heat Exchanger

of the A/C system is evaluated at the steady state. Therefore, it can be considered as the snap shot of the system working condition during the interactive and oscillatory regulation of the expansion valve.

The heat exchanger coils are divided into 30 channels in this case. Each channel consists of 12 tubes in each air passage section. The refrigerant evenly flows into each channel, thus the mass flow rates in each channel are at the same level.

Figure 24 compares the COP of the ideal case 1 and case 2 with the maldistribution of air flow. Due to the maldistribution (uneven distribution) of air flow, refrigerant in some coils does not get completely evaporated because of the low air velocity and completes superheated half-way in the passages for some other coils because of the high air velocity, which results in the loss of cooling capacity. based on the energy conservation principles, the more damaging effect of air flow maldistribution is that, the mixture of the unevaporated liquid refrigerant and the superheated vapor is a refrigerant with low superheated vapor. Responding to the state of the refrigerant (low superheated vapor) exiting from the evaporator, the expansion valve shrinks to reduce the mass flow rate of the refrigerant in order to reach an ideal and pre-set superheating temperature at the exit of the evaporator.

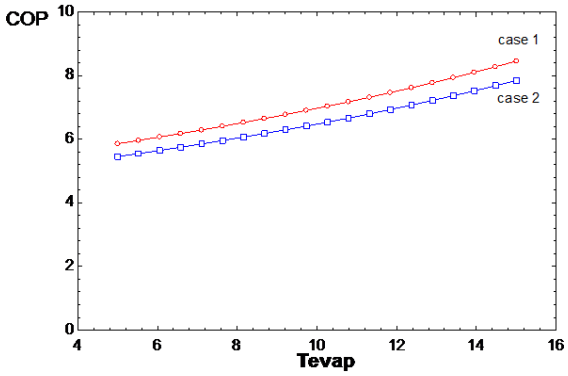

Figure 24. COP- T_{evap} Plot of Case 1 and Case 2

Thus mass flow rate is reduced and consequently, cooling capacity is decreased. For the condensing temperature T_{cond} of 45°C and targeted superheating temperature T_{suph} of 10°C, the reduction of the COP values is in the range of 6.98% at an evaporating temperature T_{evap} of 5°C to 7.21% with the evaporating temperature of 15°C. Figure 25 shows the cooling capacity, Q_L, of the ideal case 1, as compared with the results of case 2. Similar to Figure 24, the cooling capacity of the A/C systems has a decrease of about 3.45% to 3.91%. The designed A/C system under the certain temperature conditions shown in Table 1 is marked as case 2. The calculation results under these settings are as follows: Cooling capacity Q_L=43.69[kW]; Compressor Work $W_{compressor}$=8.012[kW]; Coefficient of performance COP=5.453

Compared to case 1, COP drops 6.98% and cooling capacity drops 3.43% due to air maldistribution.

4.2.3 Effects of air velocity at the entrance

The inlet speed of air into the air space is controlled by the centrifugal fan installed at the top of the evaporator. For normal operating conditions, the velocity value at the entrance is set to be 7.4 m/s, which is a boundary condition input in all previous CFD simulations. Figures 26 to 28 show the results of CFD simulations with the inlet velocity equal to 15 m/s.

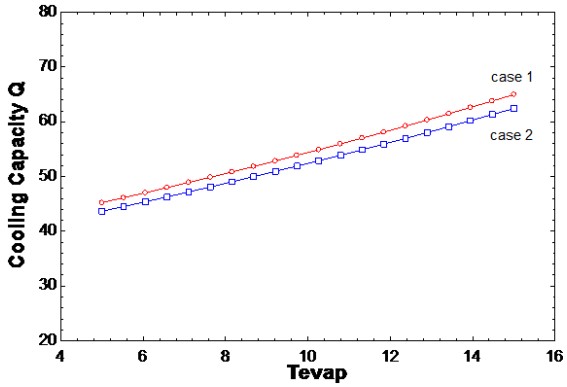

Figure 25. Q_L- T_{evap} Plot of Case 1 and Case 2

Figure 26 presents the distribution of pressure field inside the air space of the evaporator. The contours of the pressure distribution are almost identical as Figure 20, with the pressure value increased by about 300%.

Figure 27 shows the velocity distribution inside the air space of the evaporator. Figure 28 shows the velocity distribution along the heat exchanger passages. Compared to Figure 22 the speed of air through each channel increases and the air flow distribution parameter, F_{air}, decreased from 1 to approximately 0.4 for each passage along the heat exchanger in Figure 28. In other words, the maldistribution of air becomes more severe by increasing the inlet speed.

4.3 Proposed solutions

The expansion valve will work incorrectly when the refrigerant in some coils is overheated while the refrigerant in other coils does not evaporate completely. To remedy the problem, two solutions are proposed. One is to redesign the length of the evaporator channels, and change the flow resistance of the channel so that the patterns of the refrigerant distribution match the patterns of the maldistributed air flow, as 4.3.1 demonstrates. The higher flow rate, due to lower flow resistance at the shorter channels, will be allocated in regions with higher mean air velocity, and vice-versa. The other approach is to install mini controllers to the system

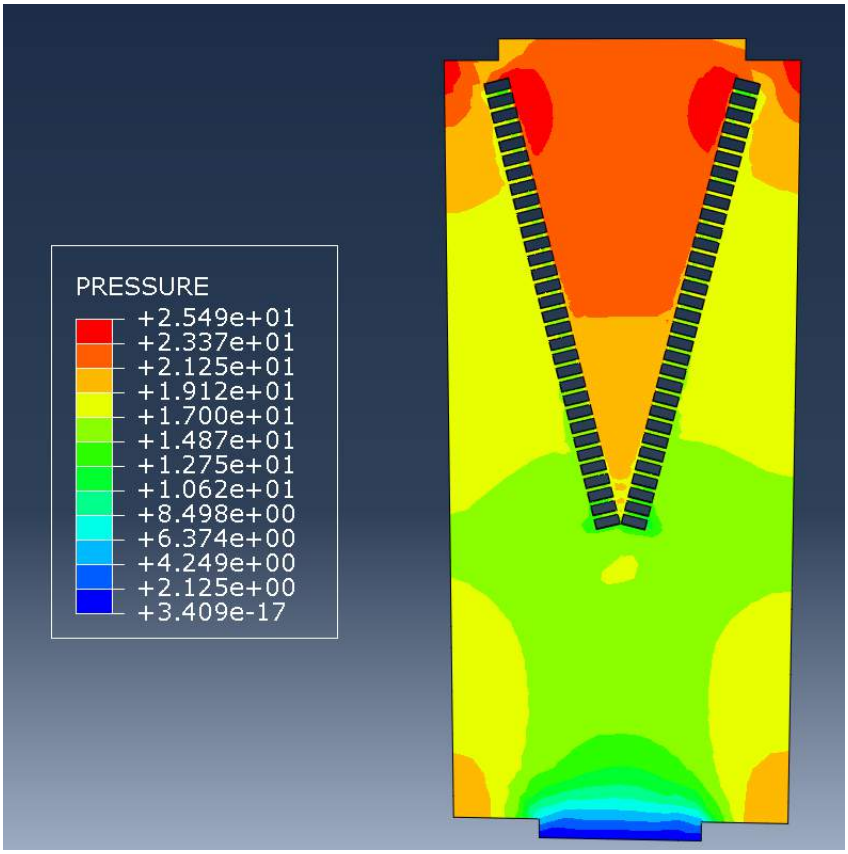

Figure 26. Pressure Distribution of Air inside the Air Space of the Evaporator with a Higher Inlet Speed

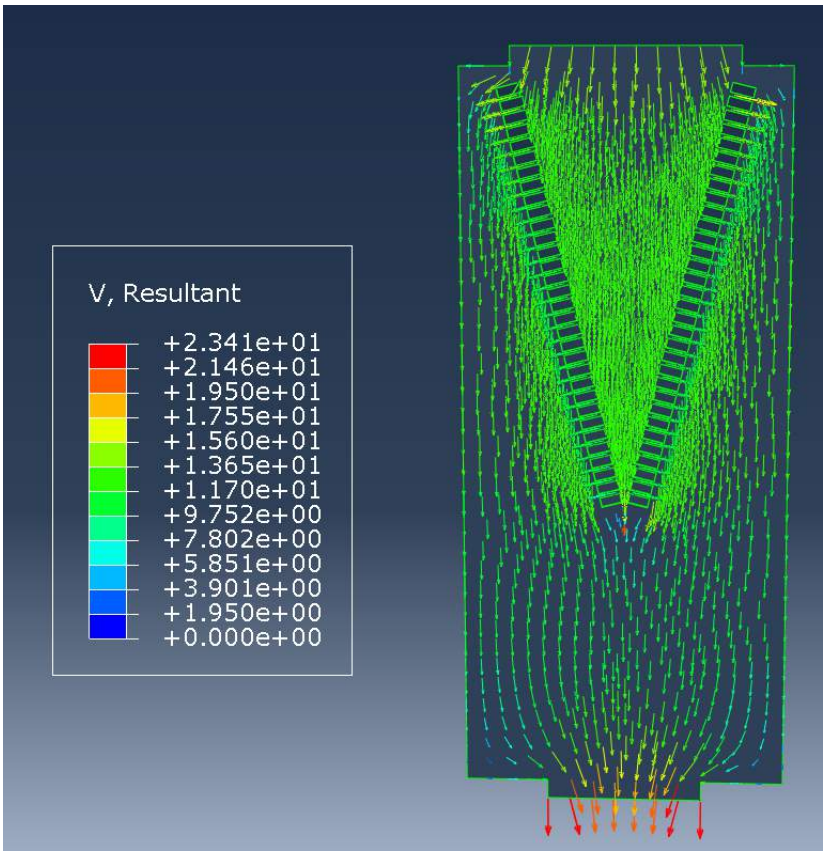

Figure 27. Velocity Distribution of Air inside the Air Space of the Evaporator with a Higher Inlet Speed

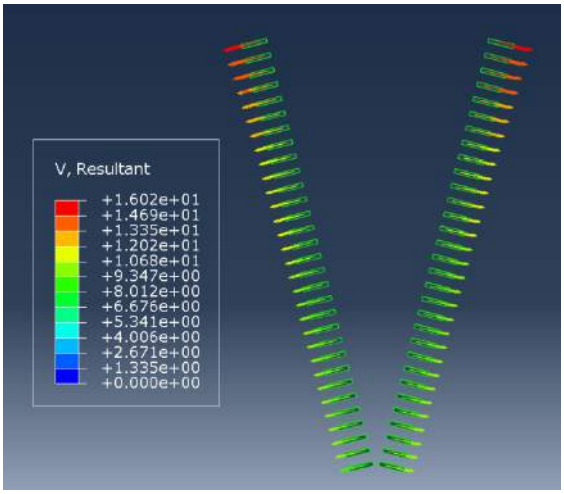

Figure 28. Velocity Distribution of Air through the Passages along the Heat Exchangers with a Higher Inlet Speed

at the exit of the refrigerant distributor to control the ratio of refrigerant flowing into each individual channel, and to ensure that all of the refrigerant exiting from each channel reaches an ideal state with the appropriate superheating, as 4.3.2 demonstrates.

The second type of strategy is to minimize the maldistribution of air from the very beginning. The increase of resistance to air flow would affect the coils with higher air velocity more than those with lower air velocity. Therefore, the modifications in the air space of the evaporator aim to increase the resistance to airflow through each coil and improve performance, as 4.3.3 and 4.3.4 demonstrates.

4.3.1 Rearrangement of Evaporator Channels

The heat exchanger coils are rearranged into 30 new channels in this case. The number of tubes in the first 5 channels reduces from 12 to 10 and the number of tubes in the last 5 channels increases from 12 to 14. There is no change of tubes in the rest of the 20 channels. The refrigerant evenly flows into each channel, thus the mass flow rates in each channel are at the same level.

The COP of the ideal case 1, the air-maldistributed case 2 without any improvements, and the air-maldistributed case 3 with rearrangement of channels as a function of the evaporating temperature, T_{evap}, are shown in Figure 29. The figure indicates that the rearrangement of coils enhance the COP moderately from case 2.

The cooling capacity, Q_L, of the ideal case 1, the air-maldistributed case 2 without any improvement, and the air-maldistributed case 3 with rearrangement of channels as a function of the evaporating temperature, T_{evap}, are shown in Figure 30. The figure indicates that the rearrangement of coils brought some recovery for the cooling capacity from case 2, but the effect was not significant. This is because the uneven distribution of the air flow is most severe near the entrance of

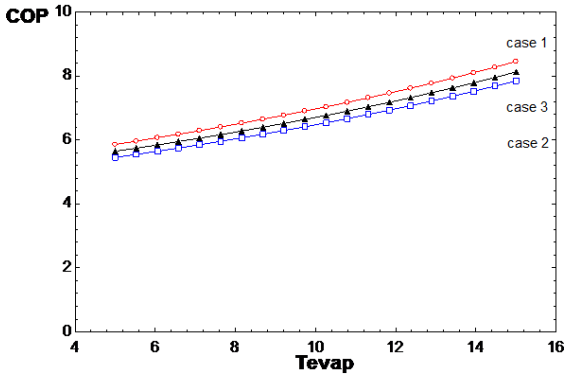

Figure 29. COP- T_{evap} Plot of Case 1-3

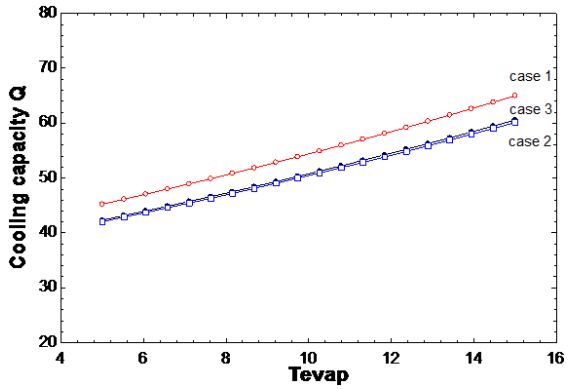

Figure 30. Q_L- T_{evap} plot of case 1-3

the air space. Therefore, the modification of the air flow channel is limited only to those channels. The designed A/C system with channels rearranged under the specific temperature conditions shown in Table 1 is marked as case 3. The calculation results under these settings are as follows: Cooling capacity Q_L=44.25[kW]; Compressor Work $W_{compressor}$=7.889[kW]; Coefficient of performance COP=5.61.

Compared to case 2, COP recovers 2.68% of the original 6.98% decrease and cooling capacity recovers 1.24% of the original 3.43% decrease due to air maldistribution.

4.3.2 Installment of Controllers on Distributor

Figure 31 shows the distribution of mass flow rate in each channel governed by the controllers as a function of the heat absorption ability of each channel. The

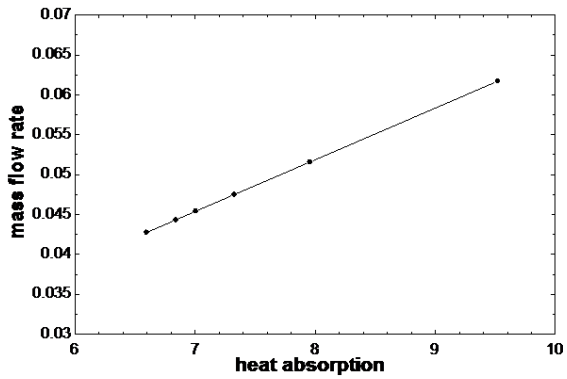

Figure 31. Distribution of Mass Flow Rate along the Heat Absorption in Each Channel

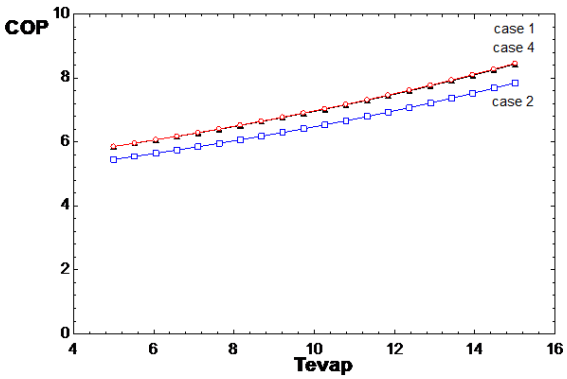

Figure 32. COP- T_{evap} Plot of Case 1, 2 and 4

figure indicates that the mass flow rate controlled in each channel is linearly dependent on the heat absorption ability of the channel determined by the velocity of airflow. The COP of the ideal case 1, the air-maldistributed case 2 without any improvement, and the air-maldistributed case 4 with a controlling theme as a function of the evaporating temperature, T_{evap}, are shown in Figure 32. The figure indicates that the installment of controllers brings considerable recovery for the COP from case 2. The cooling capacity Q_L of the ideal case 1, the air-maldistributed case 2 without any improvement, and the air-maldistributed case 4 with with a controlling theme as a function of the evaporating temperature, T_{evap}, are shown in Figure 33. Similarly to Figure 32, Figure 33 indicates that the rearrangement of coils brought almost full recovery for the cooling capacity from case

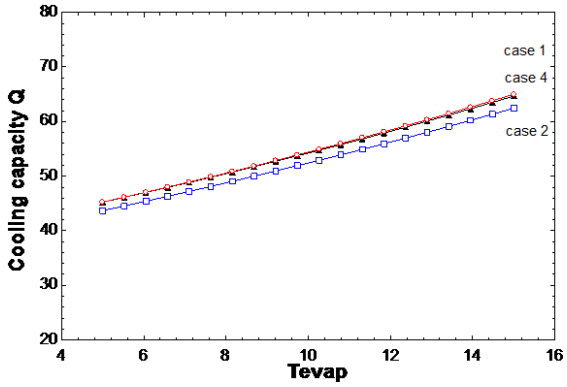

Figure 33. Q_L- T_{evap} Plot of Case 1, 2 and 4

2. The designed A/C system with control of refrigerant mass flow rate under the specific temperature conditions shown in Table 1 is marked as case 4. The calculation results under these settings are as follows: Cooling capacity Q_L=45.24[kW]; Compressor Work $W_{compressor}$=7.717[kW]; Coefficient of performance COP=5.862.

Compared to case 2, COP recovered all the 6.98% of the original 6.98% decrease and cooling capacity recovered all the 3.43% of the original 3.43% decrease due to air maldistribution. The contribution of the method is significant.

The precise control of the mass flow rate of refrigerant flowing into each channel can be achieved by applying an extra expansion valve to each channel or by installing a digital controlling scheme to the distributor. Both approaches would incredibly increase the cost of the A/C system due to high price of the expansion valves and high-precision control scheme. However, the rearrangement of the channels does not require extra devices since that it only requires to disassemble and to reassemble some of the connectors of the heat exchanger tubes. Briefly the better solution comes with a higher cost.

4.3.3 Installment of Filter Nets on the Heat Exchanger Surface

A practical approach to change air flow patterns along the evaporator surfaces is to install a layer of high flow resistance material, such as the filter nets over the

surface of the heat exchangers. The higher the air velocity is, the greater the air flow resistance would be. Thus the filter structure creates smart and adaptive resistance to air flows, particularly at the entrance where air velocity is higher. The designed A/C system with installment of filter nets on the heat exchangers is marked as case 5.

Figure 34 presents the pressure field inside the air space of the evaporator. It is clearly shown that the pressure distribution became much more even than the original case design without the filter structure.

Figure 35 shows the velocity distribution inside the air space of the evaporator with the installation of the filter structure.

Figure 36 shows the velocity distribution along the heat exchanger air passage. The air flow distribution parameter, F_{air}, decreases from 1 to approximately 0.85 for each passage along the heat exchanger. The level of the maldistribution of air flow is greatly decreased.

It is noted that an air filter is a necessary and required component for an A/C system. Typical locations of the air filter are at the entrance. Case 5 shows that installing the filter at the surface of the evaporator is a practical and feasible approach to achieve two purposes with one design.

4.3.4 Installment of a Diverter in the Evaporator Air Space

Another design approach to even the airflow distribution is to install an air diverter in the entrance region of the air space. This design forces the incoming air to flow first through the pre-designed narrower paths of the diverter to achieve a more even distribution before it flows through the heat exchangers. The designed A/C system with installment of a diverter in the evaporator air space is marked as case 6.

Figure 37 presents the pressure field inside the air space of the evaporator. It

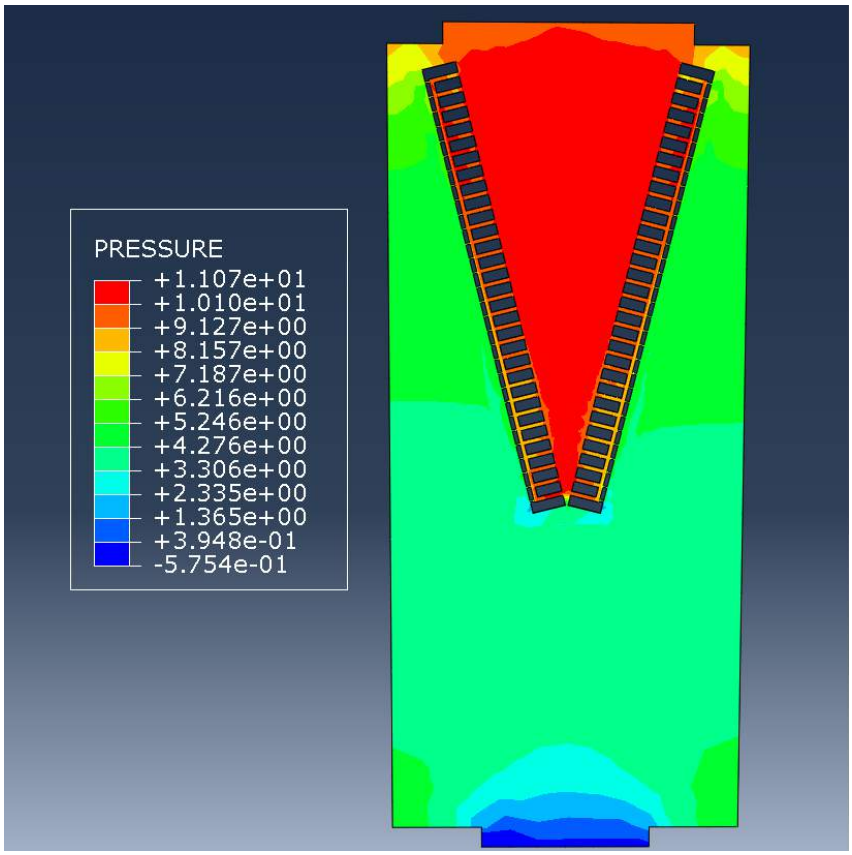

Figure 34. Pressure Distribution of Air inside the Air Space of the Evaporator in Case 5

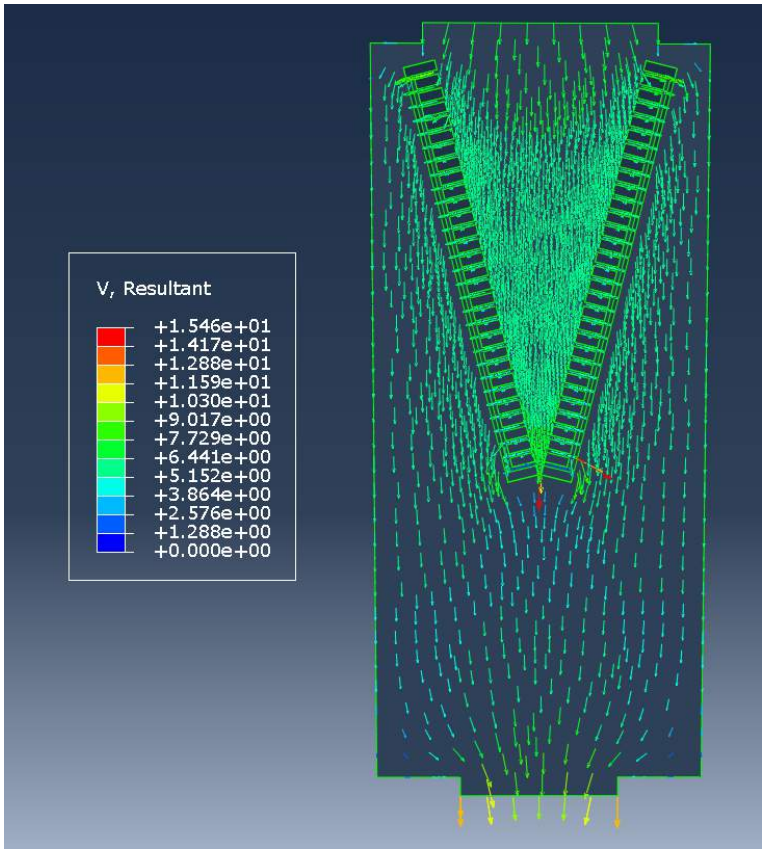

Figure 35. Velocity Distribution of Air inside the Air Space of the Evaporator in Case 5

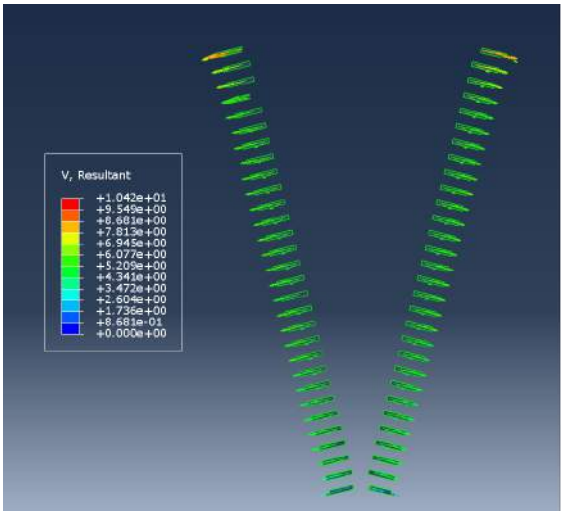

Figure 36. Velocity Distribution of Air through the Passages along the Heat Exchangers in Case 5

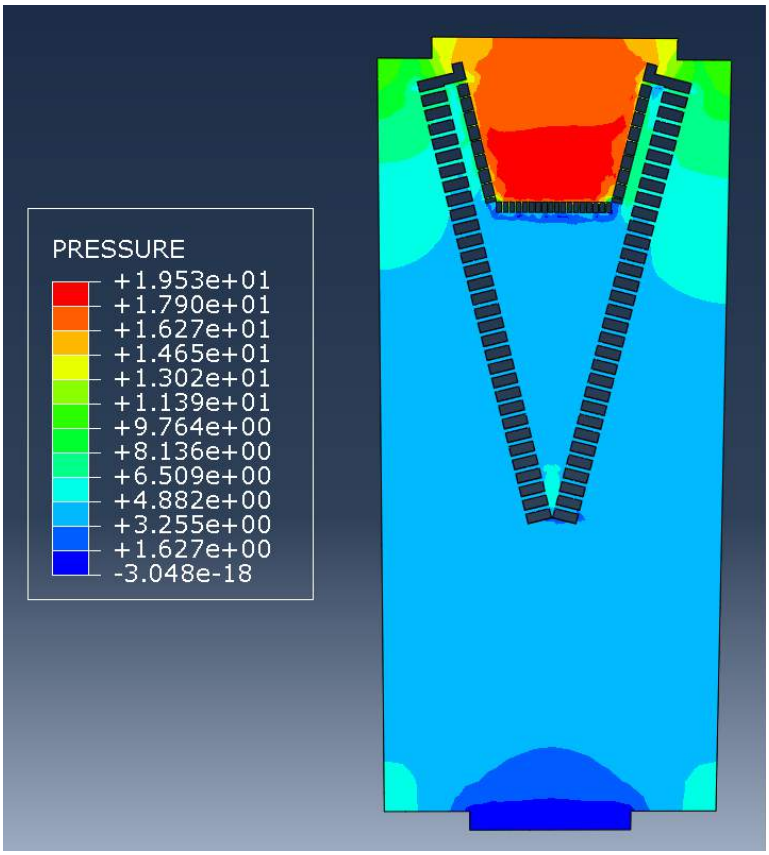

Figure 37. Pressure Distribution of Air inside the Air Space of the Evaporator in Case 6

is clearly shown that the pressure drops across the coils are more even than the original case.

Figure 38 shows the velocity distribution inside the air space of the evaporator.

Figure 39 shows the velocity distribution of air through the passages along the heat exchange. The air flow distribution parameter, F_{air}, decreases from 1 to approximately 0.83 for each coil along the heat exchanger. The level of the maldistribution of air flow is again greatly decreased.

4.4 Experimental Results

The temperature distribution of refrigerant can be measured by observing the infrared picture of the refrigerant inside the channel. The dark blue color

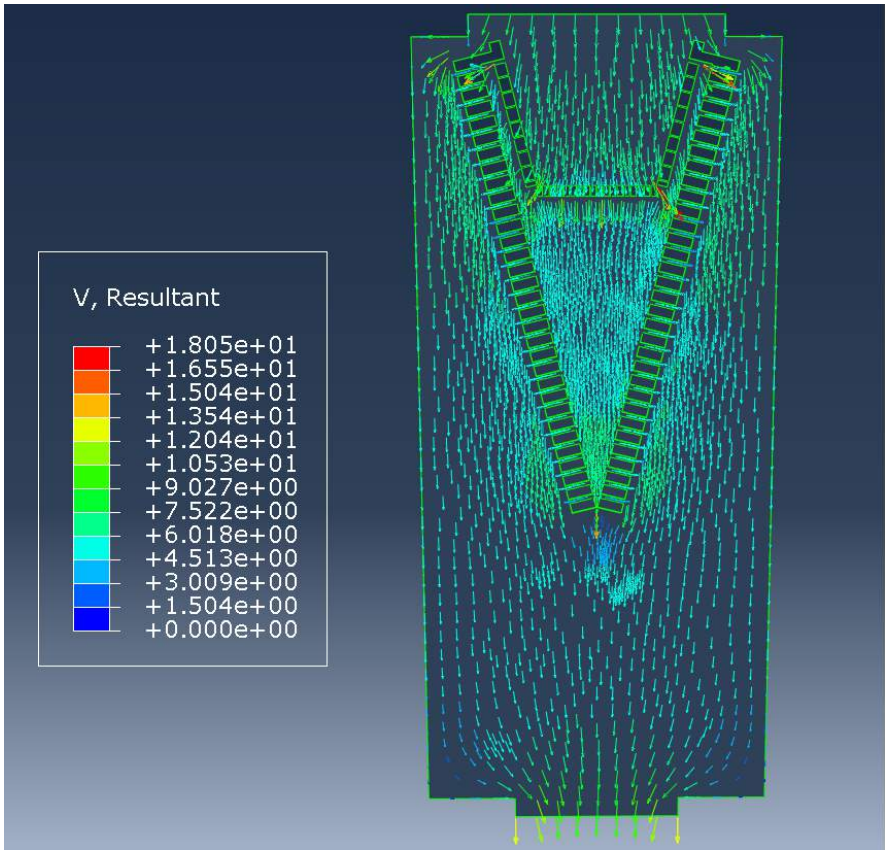

Figure 38. Velocity Distribution of Air inside the Air Space of the Evaporator in Case 6

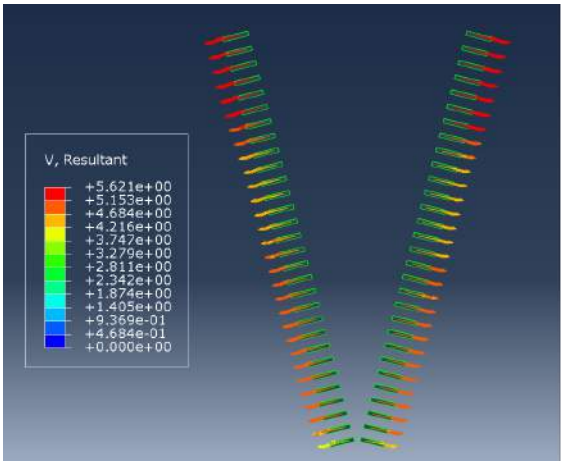

Figure 39. Velocity Distribution of Air through the Passages along the Heat Exchangers in Case 6

indicates a lower temperature of liquid and the light blue to bright blue colors represent higher temperatures of gradually superheated vapors. Two tests have been conducted. Test 1 is conducted on the original V-shaped design, as case 2 introduced in 4.2. Test 2 is conducted on the V-shaped design with an installment of filter nets, as case 5 introduced in 4.3.

Figure 40 shows the infrared picture of the evaporator of Test 1. It is shown that the refrigerant in the upper channels has a higher temperature than the one in lower channels. This indicates that the refrigerant is superheated inside the lower channels, which are subjected to higher mean air velocities, and is still in the state of vapor-mixture inside the higher channels, which are subjected to lower mean air velocities. It is noted that air enters the V-shaped evaporator through the bottom. The result reverses the conclusion of previous simulations due to the change of the design that the location of the centrifugal fan is moved from the top to the bottom of the evaporator.

Figure 41 shows the infrared picture of evaporator of Test 2. It is shown that the refrigerant temperatures are evenly distributed from the top to the bottom, which indicates that the airflow maldistribution is compensated by the design. However, it is also noted that the temperature in the left heat exchanger is lower than the temperature in the right one, which indicates that the refrigerant is not uniformly distributed symmetrically. The result is possibly caused by the refrigerant maldistribution from the distributer and this phenomenon will be studied in the future.

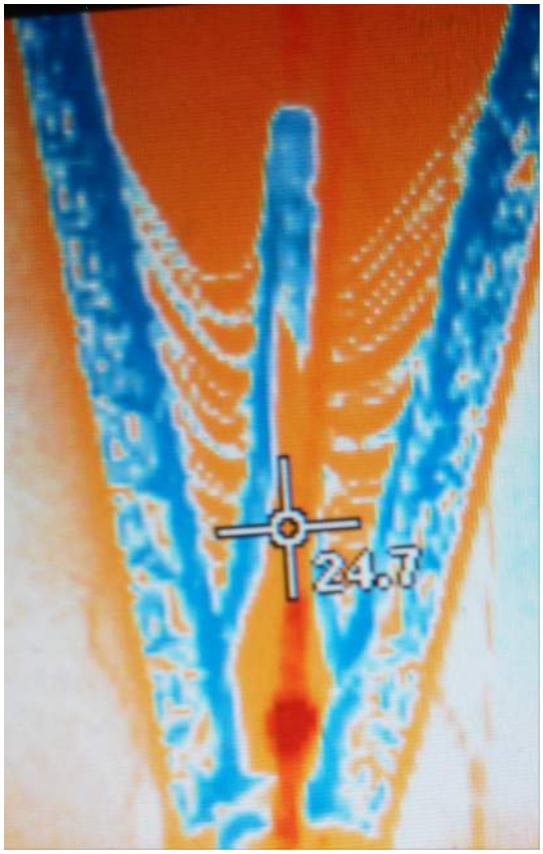

Figure 40. Infrared Camera Result of Test 1

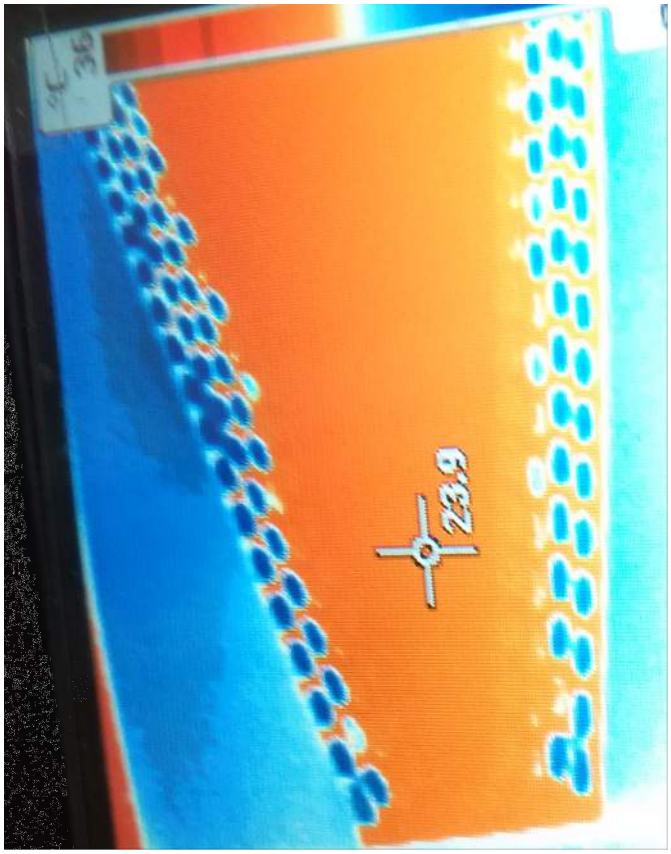

Figure 41. Infrared Camera Result of Test 2

CHAPTER 5

Conclusions and Future Work

5.1 Conclusions

A computational model of an A/C system equipped with the Model CAD501 prototype evaporator is developed. It can be concluded that airflow maldistribution in the V-shaped prototype evaporator with a multiple-channel design reduces the cooling capacity and coefficient of performance of the A/C system. Four feasible approaches are proposed in this work, which could significantly compensate the airflow maldistribution in terms of cooling capacity and coefficient of performance.

Six cases are studied in this work, i.e. case 1 an ideal case without airflow maldistribution, case 2 the original case with airflow maldistribution, case 3 the compensated case with a rearrangement of channels, case 4 the compensated case with control theme, case 5 the compensated case with installment of filter nets, and case 6 the compensated case with installment of an air diverter. Compared to case 1, case 2 shows a 3.45% and 6.77% degradation in cooling capacity and coefficient of performance. Compared to case 2, case 3 shows a 1.11% and 3.12% recovery in cooling capacity and coefficient of performance. Compared to case 2, case 4 shows a full recovery in cooling capacity and coefficient of performance. Compared to case 2, case 5 and case 6 show regulations of the airflow velocity profile.

5.2 Future Work

In general, our future work will include the following parts:

1. Optimize the modeling of the prototype evaporator, specifically, develop a 3-D model;

2. Investigate the refrigerant maldistribution caused by other factors, e.g. maldistribution from the distributer.

With the limitations of the computation abilities by the student version of ABAQUS and the lab computer, the model developed in this work is extremely simplified. A more precise model can be developed with a commercial version of the software and a more powerful computer.

Since the main focus of this study is the effect of airflow maldistribution, the distributor and other components of the A/C system are considered ideal. Further modeling of these components can contribute more details of the refrigerant in the vapor-compression refrigeration cycle of the A/C system. The refrigerant maldistribution from sources other than the airflow maldistribution inside the evaporator can be studied with the further modeling.

APPENDIX

EES Code Used In This Study

A.1 Benchmark Calculation

```
{Constants}
Tsubc=5
Tsuph=10
Tevap=5
Tcond=45
Vc=0.018
m_dot=rho*Vc
rho=Density(R134a,T=T1,P=P1)
{state 1}
T1=Tevap+Tsuph
P1=Pressure(R134a,T=Tevap,x=1)
S1=Entropy(R134a,T=T1,P=P1)
h1=Enthalpy(R134a,T=T1,P=P1)
{state 2}
S2=S1
P2=Pressure(R134a,T=Tcond,x=1)
h2=Enthalpy(R134a,P=P2,S=S2)
{state 3}
P3=P2
T3=Tcond-Tsubc
h3=Enthalpy(R134a,T=T3,P=P3)
{sate 4}
```

```
h4=h3
Q_dot=m_dot*(h1-h4)
W_compressor=m_dot*(h2-h1)
COP=Q_dot/W_compressor
```

A.2 Benchmark Plot

```
{Constants}
Tsubc=5
Tsuph=10
Tevap=5
Tcond_1=35
Tcond_2=45
Tcond_3=55
Vc=0.018
m_dot=rho*Vc
rho=Density(R134a,T=T1,P=P1)
{state 1}
T1=Tevap+Tsuph
P1=Pressure(R134a,T=Tevap,x=1)
S1=Entropy(R134a,T=T1,P=P1)
h1=Enthalpy(R134a,T=T1,P=P1)
{state 2}
S2=S1
P2_1=Pressure(R134a,T=Tcond_1,x=1)
h2_1=Enthalpy(R134a,P=P2_1,S=S2)
P2_2=Pressure(R134a,T=Tcond_2,x=1)
h2_2=Enthalpy(R134a,P=P2_2,S=S2)
```

```
P2_3=Pressure(R134a,T=Tcond_3,x=1)
h2_3=Enthalpy(R134a,P=P2_3,S=S2)
{state 3}
P3_1=P2_1
T3_1=Tcond_1-Tsubc
h3_1=Enthalpy(R134a,T=T3_1,P=P3_1)
P3_2=P2_2
T3_2=Tcond_2-Tsubc
h3_2=Enthalpy(R134a,T=T3_2,P=P3_2)
P3_3=P2_3
T3_3=Tcond_3-Tsubc
h3_3=Enthalpy(R134a,T=T3_3,P=P3_3)
{sate 4}
h4_1=h3_1
h4_2=h3_2
h4_3=h3_3
Q_dot_1=m_dot*(h1-h4_1)
W_compressor_1=m_dot*(h2_1-h1)
COP_1=Q_dot_1/W_compressor_1
Q_dot_2=m_dot*(h1-h4_2)
W_compressor_2=m_dot*(h2_2-h1)
COP_2=Q_dot_2/W_compressor_2
Q_dot_3=m_dot*(h1-h4_3)
W_compressor_3=m_dot*(h2_3-h1)
COP_3=Q_dot_3/W_compressor_3
```

A.3 Case 2

```
{Constants}
Tsubc=5
Tcond=45
Tevap=5
Vc=0.018
m_dot_1=rho*Vc
rho=Density(R134a,h=h1,P=P1)
{Inside evaporator}
r=SUM(v[i],i=1,30)/30
h1_ideal=262.5
Q_0=m_dot_1*(h1_ideal-h4)
k=Q_0/r/30
duplicate i=1,30
        q[i]=k*v[i]
end
h1_max=267
q_max_1=m_dot_1/30*(h1_max-h4)
q_max_2=m_dot_2/30*(h1_max-h4)
{Coil arrangement}
duplicate i=1,30
        Y[i]=IF(q[i],q_max_1,q[i],q_max_1,q_max_1)
end
duplicate i=1,30
        Z[i]=IF(q[i],q_max_2,q[i],q_max_2,q_max_2)
        r[i]=Z[i]/q[i]
end
```

```
Q_dot_1=SUM(Y[i],i=1,30)
Q_dot_2=SUM(Z[i],i=1,30)
{Each Channel}
duplicate i=1,30
        Y[i]=m_dot_1/30*(ha[i]-h4)
end
duplicate i=1,30
        Z[i]=m_dot_2/30*(hb[i]-h4)
end
{state 1}
P1=Pressure(R134a,T=Tevap,x=1)
S1=Entropy(R134a,h=h1,P=P1)
T1=Temperature(R134a,h=h1,P=P1)
{state 2}
S2=S1
P2=Pressure(R134a,T=Tcond,x=1)
h2=Enthalpy(R134a,P=P2,S=S2)
{state 3}
P3=P2
T3=Tcond-Tsubc
h3=Enthalpy(R134a,T=T3,P=P3)
{sate 4}
h4=h3
Q_dot_1=m_dot_1*(h1-h4)
W_compressor_1=m_dot_1*(h2-h1)
COP_1=Q_dot_1/W_compressor_1
```

```
{After expansion valve}
{state 1}
h1_a=h1_ideal
h1_a=SUM(hb[i],i=1,30)/30
S1_a=Entropy(R134a,h=h1_a,P=P1)
T1_a=Temperature(R134a,h=h1_a,P=P1)
{state 2}
S2_a=S1_a
h2_a=Enthalpy(R134a,P=P2,S=S2_a)
W_compressor_2=m_dot_1*(h2_a-h1_a)
COP_2=Q_dot_2/W_compressor_2
```

A.4 Case 3

```
{Constants}
Tsubc=5
Tcond=45
Tevap=5
Vc=0.018
m_dot_1=rho*Vc
rho=Density(R134a,h=h1,P=P1)
{Inside evaporator}
r=SUM(v[i],i=1,30)/30
h1_ideal=262.5
Q_0=m_dot_1*(h1_ideal-h4)
k=Q_0/r/30
duplicate i=1,30
        q[i]=k*v[i]
```

```
end
h1_max=267
q_max=m_dot_1/30*(h1_max-h4)
q_max_2=m_dot_2/30*(h1_max-h4)
{Coil arrangement}
duplicate i=1,4
        Y[i]=IF(q[i]*10/12,q_max,q[i]*10/12,q_max,q_max)
        Z[i]=IF(q[i]*10/12,q_max_2,q[i]*10/12,q_max_2,q_max_2)
end
duplicate i=5,26
        Y[i]=IF(q[i],q_max,q[i],q_max,q_max)
        Z[i]=IF(q[i],q_max_2,q[i],q_max_2,q_max_2)
end
duplicate i=27,30
        Y[i]=IF(q[i]*14/12,q_max,q[i]*14/12,q_max,q_max)
        Z[i]=IF(q[i]*14/12,q_max_2,q[i]*14/12,q_max_2,q_max_2)
end
Q_dot_1=SUM(Y[i],i=1,30)
Q_dot_2=SUM(Z[i],i=1,30)
{Each coil}
duplicate i=1,30
        Y[i]=m_dot_1/30*(ha[i]-h4)
end
duplicate i=1,30
        Z[i]=m_dot_2/30*(hb[i]-h4)
end
```

```
{state 1}
P1=Pressure(R134a,T=Tevap,x=1)
S1=Entropy(R134a,h=h1,P=P1)
T1=Temperature(R134a,h=h1,P=P1)
{state 2}
S2=S1
P2=Pressure(R134a,T=Tcond,x=1)
h2=Enthalpy(R134a,P=P2,S=S2)
{state 3}
P3=P2
T3=Tcond-Tsubc
h3=Enthalpy(R134a,T=T3,P=P3)
{sate 4}
h4=h3
Q_dot_1=m_dot_1*(h1-h4)
W_compressor_1=m_dot_1*(h2-h1)
COP_1=Q_dot_1/W_compressor_1
{After expansion valve}
{state 1}
h1_a=h1_ideal
h1_a=SUM(hb[i],i=1,30)/30
S1_a=Entropy(R134a,h=h1_a,P=P1)
T1_a=Temperature(R134a,h=h1_a,P=P1)
{state 2}
S2_a=S1_a
h2_a=Enthalpy(R134a,P=P2,S=S2_a)
```

```
W_compressor_2=m_dot_1*(h2_a-h1_a)
COP_2=Q_dot_2/W_compressor_2
```

A.5 Case 4

```
{Constants}
Tsubc=5
Tcond=45
Tevap=5
Vc=0.018
m_dot=rho*Vc
rho=Density(R134a,h=h1,P=P1)
{Inside evaporator}
r=SUM(v[i],i=1,30)/30
h1_ideal=262.5
Q_0=m_dot*(h1_ideal-h4)
k=Q_0/r/30
duplicate i=1,30
        q[i]=k*v[i]
end
h1_max=267
q_max=m_dot/30*(h1_max-h4)
{Coil arrangement}
duplicate i=1,30
        Y[i]=IF(q[i],q_max,q[i],q_max,q_max)
end
duplicate i=1,30
        q[i]=m[i]*(h1_ideal-h4)
```

```
end
m=SUM(m[i],i=1,30)
Q_dot=SUM(q[i],i=1,30)
{state 1}
P1=Pressure(R134a,T=Tevap,x=1)
S1=Entropy(R134a,h=h1,P=P1)
{state 2}
S2=S1
P2=Pressure(R134a,T=Tcond,x=1)
h2=Enthalpy(R134a,P=P2,S=S2)
{state 3}
P3=P2
T3=Tcond-Tsubc
h3=Enthalpy(R134a,T=T3,P=P3)
{sate 4}
h4=h3
Q_dot=m_dot*(h1-h4)
W_compressor=m_dot*(h2-h1)
COP=Q_dot/W_compressor
```

BIBLIOGRAPHY

Abdelaziz, O., Singh, V., Aute, V., and Radermacher, R., "A-type heat exchanger simulation using 2-d cfd for airside heat transfer and pressure drop," 2008.

Ahamed, J., Saidur, R., and Masjuki, H., "A review on exergy analysis of vapor compression refrigeration system," *Renewable and Sustainable Energy Reviews*, vol. 15, no. 3, pp. 1593–1600, 2011.

Brix, W., Kærn, M. R., and Elmegaard, B., "Modelling refrigerant distribution in microchannel evaporators," *International Journal of refrigeration*, vol. 32, no. 7, pp. 1736–1743, 2009.

Cengel, Y. A., Boles, M. A., and Kanoğlu, M., *Thermodynamics: an engineering approach*. McGraw-Hill New York, 2011, vol. 5.

Domanski, P. A. and Yashar, D., "Application of an evolution program for refrigerant circuitry optimization," *Proc. ACRECONF" Challenges To Sustainability*, 2007.

Domanski, P. A., Yashar, D., Kaufman, K. A., and Michalski, R. S., "An optimized design of finned-tube evaporators using the learnable evolution model," *HVAC&R Research*, vol. 10, no. 2, pp. 201–211, 2004.

Groll, E., Braun, J., and Bach, C., "Optimizing refrigerant distribution in evaporators–final report," *California Energy Commission. Publication number: CEC-500-2013-089*, 2011.

Kærn, M. R., Brix, W., Elmegaard, B., and Larsen, L. F. S., "Performance of residential air-conditioning systems with flow maldistribution in fin-and-tube evaporators," *international journal of refrigeration*, vol. 34, no. 3, pp. 696–706, 2011.

Kærn, M. R. and Elmegaard, B., "Analysis of refrigerant mal-distribution: in fin-and-tube evaporators," *Danske Køledage*, pp. 25–35, 2009.

Kærn, M. R., Elmegaard, B., and Larsen, L. F. S., "Effect of refrigerant maldistribution in fin-and-tube evaporators on system performance," in *50th International Conference of Scandinavian Simulation Society*, pp. 315–322.

Kim, J., Braun, J., and Groll, E., "Optimizing refrigerant distribution in evaporators," *Final Report ARTI-06040. Air-Conditioning and Refrigeration Technology Institute, Arlington, VA, USA*, 2008.

Kim, J.-H., Braun, J. E., and Groll, E. A., "Evaluation of a hybrid method for refrigerant flow balancing in multi-circuit evaporators," *international journal of refrigeration*, vol. 32, no. 6, pp. 1283–1292, 2009.

Kim, J.-H., Braun, J. E., and Groll, E. A., "A hybrid method for refrigerant flow balancing in multi-circuit evaporators: Upstream versus downstream flow control," *international journal of refrigeration*, vol. 32, no. 6, pp. 1271–1282, 2009.

Kim, J., Braun, J. E., and Groll, E. A., "Analysis of refrigerant flow distribution in evaporators," 2008.

Klein, S. and Alvarado, F., "Ees manual," *Middleton, Wisconsin, USA*, 1999.

Koomey, J., "Growth in data center electricity use 2005 to 2010," *A report by Analytical Press, completed at the request of The New York Times*, p. 9, 2011.

Lee, J. and Domanski, P. A., "Impact of air and refrigerant maldistributions on the performance of finned-tube evaporators with r-22 and r-407c," *Final Report, ARTI MCLR Project*, no. 665-54500, 1997.

Lee, J., Kwon, Y.-C., and Kim, M. H., "An improved method for analyzing a fin and tube evaporator containing a zeotropic mixture refrigerant with air mal-distribution," *International Journal of Refrigeration*, vol. 26, no. 6, pp. 707–720, 2003.

Liu, J., Wei, W., Ding, G., Zhang, C., Fukaya, M., Wang, K., and Inagaki, T., "A general steady state mathematical model for fin-and-tube heat exchanger based on graph theory," *International Journal of Refrigeration*, vol. 27, no. 8, pp. 965–973, 2004.

Mader, G., Thybo, C., and Rasmussen, H., "An electronic expansion valve with automatic refrigerant distribution control," *Kurzfassungen. Deutsche Kälte-Klima-Tagung 2010*, 2010.

Payne, W. V. and Domański, P., *Potential Benefits of Smart Refrigerant Distributors: Final Report*. DIANE Publishing, 2002.

Rumsey, C., Smith, B., and Huang, G., "Langley research center turbulence modeling resource," *http://turbmodels. larc. nasa. gov/[retrieved 13 Nov. 2015]*, 2012.

T'Joen, C., De Paepe, M., and Vanhee, F., "Heat exchanger behavior in non uniform flow," *Experimental heat transfer*, vol. 19, no. 4, pp. 281–296, 2006.